

NPC DAB Converter for EV Charging Station

A

Thesis

*Submitted in partial satisfaction of the requirements for the
Degree of
Master of Technology*

Submitted by

Ram Gopal

(224102111)

Under the Supervision of

Dr. Chandan Kumar



Department of Electronics and Electrical Engineering

Indian Institute of Technology, Guwahati

June 2024

,

Declaration

This is to certify that the thesis entitled "**NPC-DAB converter for EV charging station**", submitted by me to the Indian Institute of Technology Guwahati, for the award of the degree of M.Tech, is a bonafide work carried out by me under the supervision of **Dr. Chandan Kumar**. The content of this thesis, in full or in parts, has not been submitted to any other University or Institute for the award of any degree.

Ram Gopal

Department of Electronics and Electrical Engineering,
Indian Institute of Technology Guwahati, Assam.

Certificate

This is to certify that the work contained in this thesis entitled "**NPC-DAB converter for EV charging station**" is a bonafide work of **Ram Gopal (Roll No. 224102111)**, carried out in the Department of Electronics and Electrical Engineering, Indian Institute of Technology, Guwahati under my supervision and it has not been submitted elsewhere for a degree.

Supervisor: **Dr. Chandan kumar**

Associate Professor,

June, 2024

Department of Electronics and Electrical Engineering,

Guwahati.

Indian Institute of Technology Guwahati, Assam.

Acknowledgements

I would like to take this opportunity to acknowledge everyone who has assisted me during this enthusiastic and enriching period of my master's program.

First and foremost, I would like to express my deepest gratitude to my project supervisor, **Dr. Chandan Kumar**, for his unwavering support and guidance throughout this project journey. I am immensely grateful to him for providing me with the opportunity to undertake this wonderful project. His dedication and work ethic will always serve as a benchmark for me.

I would also like to extend my heartfelt thanks to the Indian Institute of Technology, Guwahati, for their financial, academic, and technical support. Additionally, I am grateful to the Department of Electronics and Electrical Engineering for their support throughout this project.

My sincere appreciation goes to Somnath Meikap for his invaluable assistance. I would also like to extend my sincere thanks to all member of Smart Energy Conversion Lab for their support and encouragement throughout the project.

Sincerely

Ram Gopal

Abstract

As fuel prices continue to rise, electric vehicles (EVs) have gained popularity due to their increased efficiency, lower maintenance requirements, and reduced dependency on fossil fuels. The growing demand for sustainable mobility and the widespread adoption of EVs necessitate the establishment of an extensive and efficient charging infrastructure. To meet future EV requirements, particularly in terms of rapid charging, an advanced charging station topology is essential.

This report introduces a charging topology that employs a Neutral-Point-Clamped (NPC) converter as the first stage and a Dual Active Bridge (DAB) as the second stage. This configuration offers several advantages, including compact size and enhanced safety due to electrical isolation among all ports, making it an ideal converter topology for such applications. In this topology, the NPC converter is connected to a medium-voltage DC source through two capacitors. The output of this NPC inverter is then connected to an H-bridge, which operates as a rectifier.

The report provides a comprehensive study of the NPC DAB converter, focusing on the literature review and the printed circuit board (PCB) design of the NPC submodule for hardware development. It encompasses various phases, including open-loop simulation, close-loop simulation, and the operational details of both open-loop and close-loop hardware implementations.

Contents

1	Introduction	1
1.1	Background	2
1.1.1	Non-isolated DC-DC converter	2
1.1.2	Dual Active Bridge Converter	4
Fundamental analysis of DAB	4	
Control techniques	6	
1.1.3	Modular Multilevel Converter	7
1.1.4	What are the advantages of using the NPC-DAB converter?	9
2	Literature Survey	10
2.1	Neutral Point Clamped-Dual Active Bridge Converter	10
2.1.1	Neutral Point Diode Clamped configuration	11
2.1.2	Switching states of the 3L-NPC Bridge	11
2.1.3	Power flow equations for 5-level NPC-DAB converter	13
2.1.4	Power flow equations for 4-level NPC-DAB converter	15
3	PCB Design	17
3.1	Hardware detail of NPC submodule	18
3.1.1	Power circuit	18
3.1.2	Blanking circuit	18
3.1.3	Protection circuit	19
3.1.4	Gate driver circuit	20
3.1.5	Sensor circuit	20
3.2	PCB board layout	21
4	Simulation	23
4.1	Simulaton Setup	23
4.2	Switching Control	23
4.3	Open loop control of NPC-DAB converter	24
4.4	Close loop control of NPC-DAB converter	27
4.4.1	At R=20Ω	29

4.4.2	At R=10Ω	30
4.4.3	When R change from 20Ω to 10Ω	30
5	Hardware Setup and Result	32
5.1	Hardware Setup	32
5.1.1	NPC submodule	35
5.1.2	H Bridge Submodule	35
5.1.3	Transformer	36
5.1.4	DSP	37
5.2	Open loop control of NPC-DAB converter	38
5.3	Close Loop control of NPC-DAB converter	39
6	Conclusion and Future Scope	42
6.1	Conclusion	42
6.2	Future scope	43

List of Figures

1.1	NPC converter as DAB setup.	2
1.2	(A) Buck converter (B) Boost converter.	3
1.3	Buck-boost converter.	3
1.4	Dual active bridge Converter.	5
1.5	Waveform.	6
1.6	(a) MMC circuit (b) Half bridge submodule (c) Full bridge submodule.	8
2.1	3 level NPC-DAB converter.	10
2.2	Leg A.	12
2.3	"+" switching state.	12
2.4	"0" switching state.	12
2.5	"-" switching state.	12
2.6	Waveform of 5-level NPC-DAB Converter in all three cases.	13
2.7	Waveform of 4-level NPC-DAB Converter in all three cases.	15
3.1	Block diagram of modelled PCB.	17
3.2	Power circuit.	18
3.3	Blanking circuit.	19
3.4	Protection circuit.	20
3.5	Gate driver circuit.	20
3.6	Voltage sensor circuit.	21
3.7	PCB	22
4.1	NPC-DAB converter.	23
4.2	Switching technique for NPC-DAB converter.	24
4.3	Switching pulses for different switches.	25
4.4	Open loop simulation of 3-level NPC-DAB converter.	25
4.5	Switching control subsystem.	26
4.6	Voltage waveforms in open loop simulation for load $R = 5\Omega$	26
4.7	Current waveforms in open loop simulation for load $R = 5\Omega$	27
4.8	Close loop scheme for NPC-DAB converter.	28

4.9	Waveforms for $R = 20 \Omega$	29
4.10	Waveforms for $R = 10\Omega$	30
4.11	Waveforms for $R = 20 \Omega$ to $R = 10 \Omega$	31
5.1	Hardware schematic.	32
5.2	Full rack setup.	33
5.3	Rack PCB setup.	34
5.4	Picture of NPC submodule.	34
5.5	Picture of Sensors.	34
5.6	Picture of H Bridge PCB.	34
5.7	Picture of DSP.	34
5.8	Picture of Splited DC Supply.	35
5.9	Picture of Transformer.	35
5.10	DSP switching pulse and protection	37
5.11	DSP protection	38
5.12	Waveforms for different switches and conditions	38
5.13	Waveforms for different switches and conditions	39
5.14	(a) Primary side voltage, (b) Secondary side voltage, (c) output current	39
5.15	Close loop schematic for NPC-DAB converter.	40
5.16	Close loop scheme for single phase shift.	41
5.17	(a)Output voltage, (b)Output current.	41

List of Tables

2.1	Switching State Table.	11
4.1	Simulation parameters for open loop operation of NPC-DAB converter. .	26

Chapter 1

Introduction

Electric vehicles (EVs) are gaining popularity as the world seeks to reduce global CO₂ emissions and address the depletion of finite fossil fuel reserves. EVs, powered by battery energy storage, are replacing less efficient internal combustion engines (IC engines). However, two critical challenges facing electric vehicles are charging time and driving range. Currently, Different power converter systems are being used for electric vehicle (EV) charging stations. Generally, non-isolated converters are used in EV charging stations due to their easy control and low cost. Conventional off board EV fast charging stations generally neglect the requirement of isolation of EV [1, 2]. However, isolation is important for device protection, especially during adverse operating conditions like high voltage transients, high current transients due to faults in the grid, etc. [3].

Recently with the advancement of SiC-based switches and transformer core materials, there has been a rise in the use of isolated converter systems such as dual active bridge [4]. These converters are commonly proposed for different applications like renewable integration with energy storage systems and LVDC microgrids, and they are also an integral part of solid state transformers [5, 6]. While these converters offer advantages like isolation, they have drawbacks such as limited fault tolerance and reduced voltage levels (compared to 3-level and 5-level converters). So, we can use the multilevel modular converter. With the combination of many MMCs, we can develop many topologies such as dual active bridge, triple active bridge, quad active bridge, 3 level converter, 5 level converters etc. [7]. Although it has versatile use it is very costly and has a complex design. To strike a balance between complexity and functionality, a NPC-DAB converter has been proposed. It has a

simple design and simple control and it has not been explored in the field of EV charging stations properly [8].

In the second section of this chapter, we will delve into the background of various converter technologies. We will begin by examining non-isolated DC-DC converters, providing an overview of their design and applications. Following this, we will explore the Dual Active Bridge (DAB) converter, discussing its principles and advantages. Subsequently, we will focus on the Modular Multilevel Converter (MMC), highlighting its structure and operational benefits. Finally, we will explain the rationale behind using the Neutral Point Clamped Dual Active Bridge (NPC-DAB) converter.

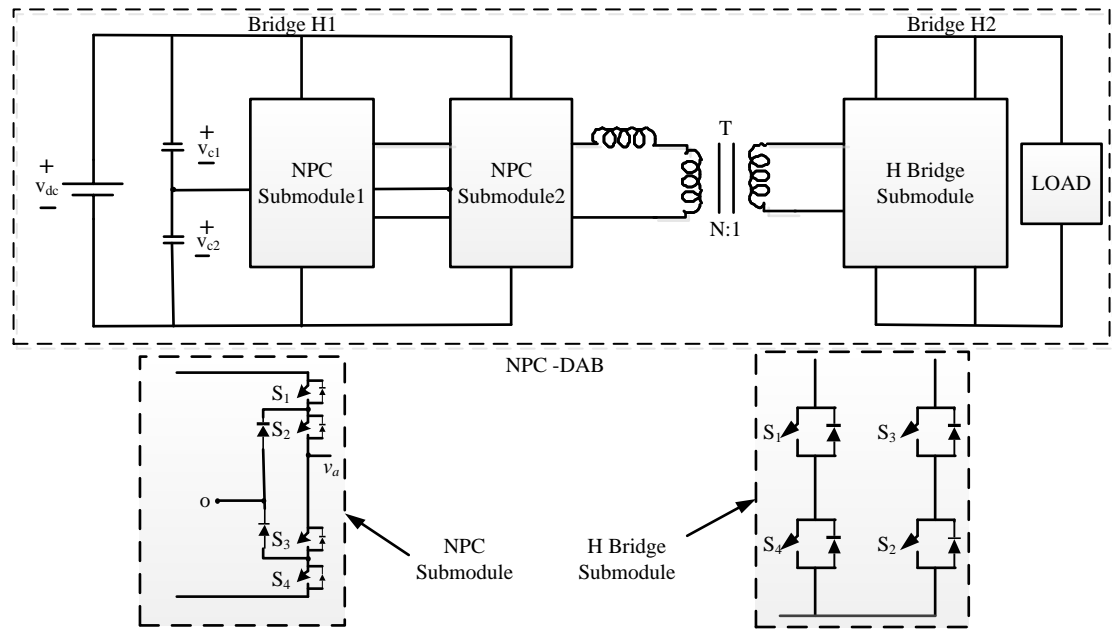


Figure 1.1: NPC converter as DAB setup.

1.1 Background

1.1.1 Non-isolated DC-DC converter

A DC-DC converter is an electronic circuit or device that transforms one level of direct current (DC) voltage into another. These converters are widely used in various applications to efficiently control and regulate DC voltage levels. DC-DC converters are crucial in various applications, such as power supplies for electronic devices, renewable energy systems, battery-powered devices, and electric vehicles. They play a key role in efficiently

managing and distributing electrical power in modern electronics. The choice of a specific DC-DC converter depends on the application's power requirements, efficiency considerations, and the desired voltage transformation characteristics. There are several types of DC-DC converters, each with its own characteristics and applications. Some common types are buck converter, boost converter, and buck-boost converter. Those are shown in fig. 1.2 and 1.3.

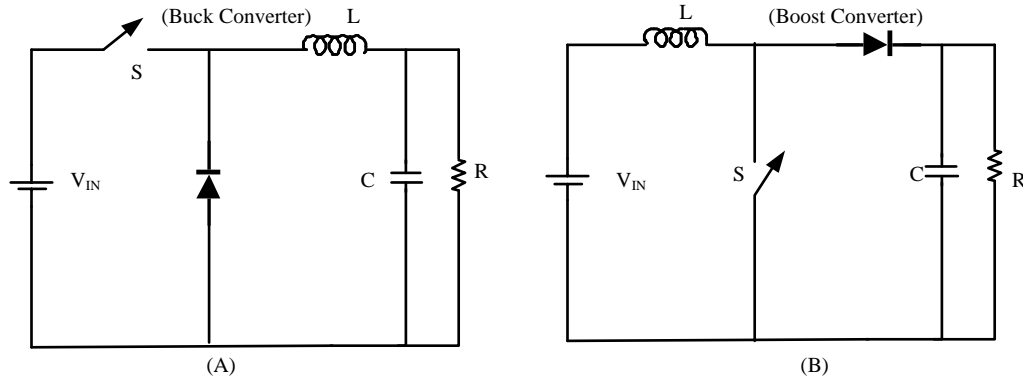


Figure 1.2: (A) Buck converter (B) Boost converter.

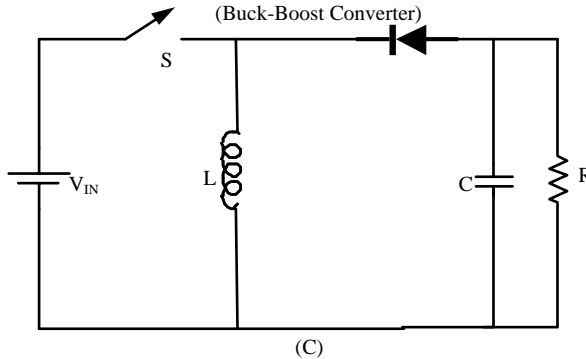


Figure 1.3: Buck-boost converter.

Advantage:

- **Voltage Regulation:** DC-DC converters provide precise control over the output voltage, ensuring a stable and regulated supply.
- **Voltage Transformation:** DC-DC converters enable the transformation of DC voltage from one level to another. This ability to step up (boost), step down (buck), or perform both functions (buck-boost) is valuable for adapting power sources to meet specific requirements in different parts of a system.

- **Improved Battery Management:** In battery-powered systems, DC-DC converters contribute to effective battery management by optimizing the use of available energy and ensuring that devices receive the required voltage levels.

Limitation:

- **Voltage Ripple:** DC-DC converters may introduce higher voltage ripple on both input and output sides. This ripple can affect the performance of sensitive electronic components and may require additional filtering.
- **Non-Isolated:** Basic DC-DC converters are typically non-isolated, which means there is no electrical separation between the input and output. In applications requiring isolation, additional components such as transformers or optocouplers may be necessary.

1.1.2 Dual Active Bridge Converter

A Dual Active Bridge (DAB) converter is a bidirectional DC/DC converter in which both the input and output voltages are in DC form. It leverages two identical H-bridge configurations on the primary and secondary sides, along with a high-frequency isolating transformer. The DAB converter incorporates active devices on both the input and output sides, resulting in a compact and efficient topology that minimizes the need for additional reactive components. It also ensures low stress on the devices and efficiently utilizes the transformer's leakage inductance as the primary energy transfer element. When power is flowing from the DC side to the converter, this circuit acts as an inverter and then it feeds it to the transformer and the transformer to the second part of the circuit, the second half of the circuit behaves like a rectifier, we are using a high-frequency transformer for high efficiency with electrical insulation. One major advantage of such a converter is the bidirectional power flow and ability to control the reactive power of the Grid.

Fundamental analysis of DAB

$$V_{a1} = V_1 \angle \Delta_1 V_{b1} = V_2 \angle \Delta_2 \quad (1.1)$$

$$I_1 = \frac{V_1 \angle \Delta_1 - V_2 \angle \Delta_2}{xL \angle 90} \quad (1.2)$$

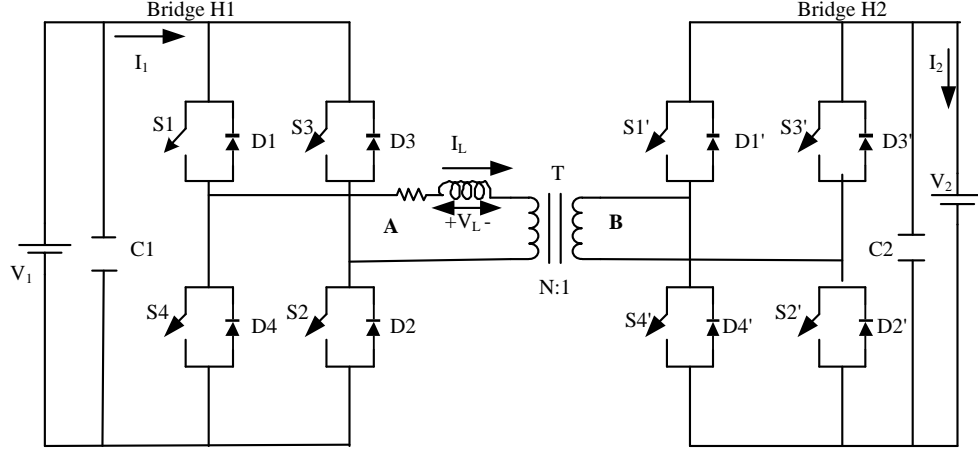


Figure 1.4: Dual active bridge Converter.

$$I_1 = \frac{V_1 \angle(\Delta_1 - 90)}{xL} - \frac{V_2 \angle(\Delta_2 - 90)}{xL} \quad (1.3)$$

If a single frequency is present then

$$S = V_o * (I_O)^*, P = VI \cos\theta, Q = VI \sin\theta \quad (1.4)$$

$$S = P + iQ \quad (1.5)$$

$$S = V_2 \angle \Delta_2 * (I_1)^* \quad (1.6)$$

$$S = V_2 \angle \Delta_2 * \left(\frac{V_1 \angle(\Delta_1 - 90)}{xL} - \frac{V_2 \angle(\Delta_2 - 90)}{xL} \right)^* S = \left(\frac{V_1 * V_2 \angle(90 - \Delta_1 + \Delta_2)}{xL} - \frac{(V_2)^2 \angle 90}{xL} \right) \quad (1.7)$$

$$P_L = \frac{V_1 * V_2 * \cos(90 - (\Delta_1 - \Delta_2))}{xL} \quad (1.8)$$

$$P_L = \frac{V_1 * V_2 * \sin(\Delta_1 - \Delta_2)}{xL} \quad (1.9)$$

$$Q_L = \frac{V_1 * V_2 * \cos(\Delta_1 - \Delta_2)}{xL} - \frac{(V_2)^2}{xL} \quad (1.10)$$

From equation (1.9) we can see that for power to flow from a to b there must be a phase difference between V_p and V_s and hence switching pulses of two H-bridges must have a phase difference. This phase shift controls the amount of power flow.

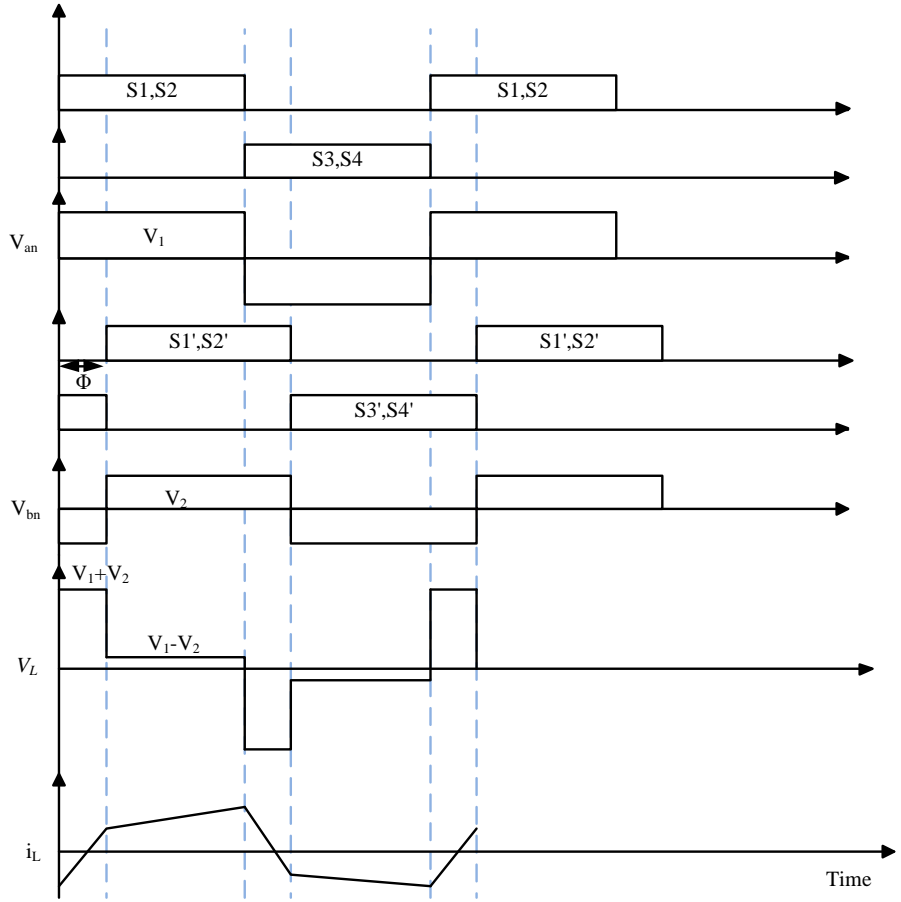


Figure 1.5: Waveform.

Control techniques

In control techniques, we mainly control the phase shift between the output voltages of two bridge converters so the power flow can be possible from the leakage inductance of the transformer as we know that in an AC system power flow from one end to the other end when it is changed in voltage angle.

Single Phase Shift (SPS) In the single-phase shift control technique, in converter 1, the opposite leg switches into conduction mode. We apply the phase shift in the 2nd bridge converter for the power flow from one end to the other end. This technique is considered the easiest and most usable in DAB. However, a disadvantage is that power flow depends on leakage inductance, causing circulating current. As a result, we cannot achieve the full range of ZVS and obtain only a 2-level output voltage. In the SPS method, the phase shift is given only between the corresponding switches of two active bridges having

gate signals with 50% duty cycle. Thus, the voltage present at the transformer terminals is a two-level AC square wave and can be modified by adjusting the phase shift. The power flowing through the converter can be regulated by controlling the current passing through the leakage inductor which depends on the voltage across the terminals of the transformer. SPS modulation is easy to implement and soft-switching can be achieved. In single-phase shift modulation, the steady state operation of DAB can be segregated into four intervals based on the operation of switches as discussed in the section Inductor current characteristics.

Advantages of DAB Converter

1. **Bidirectional Power Flow:** The DAB converter can efficiently handle power flow in both directions, making it suitable for applications such as battery charging/discharging, regenerative braking, and grid-tied systems.
2. **Isolation:** The use of a transformer provides galvanic isolation between the input and output, enhancing safety and allowing different voltage levels to be interfaced.
3. **High Current Flow:** The DAB converter is capable of handling high current flows due to its design, which is beneficial in applications requiring large power transfers.
4. **Control of Power Flow:** The phase shift control between the primary and secondary side H-bridges allows precise control over the power flow and direction, improving efficiency and dynamic response.

Limitations of DAB Converter

1. **No Fault Tolerance:** The DAB converter typically lacks inherent fault tolerance. Any failure in components such as switches, transformers, or control circuits can lead to the entire system failing.

1.1.3 Modular Multilevel Converter

MMC is a new member of the multilevel converter family, it was first proposed by Marquardt and Lesnicar in 2001. MMC is an advanced range multilevel voltage converter having immense potential in almost all types of high, medium, and low voltage applications.

MMC has excellent output performance, high modularity, low voltage and current stress on power switches, and easy scalability of submodules. It is constructed with the help of MMC submodules. Depending upon the voltage and power requirement, a number of submodules can be selected. The generalized structure of three-phase MMC is shown in Fig. 1.6(a) shows a general MMC circuit structure. Each leg consists of two arms, one upper arm and one lower arm. Each arm consists of multiple submodules, depending upon the voltage and power requirement, a number of submodules can be selected. Fig. 1.6(b) and (c) Show the structure of half and full bridge submodules. Arm inductors are kept to suppress the circulating current. The structure of submodules can be full-bridge or half-bridge based. Every submodule consists of a submodule capacitor which will be responsible for maintaining submodule voltage [9]. Following are some of MMC's advantages and limitations.

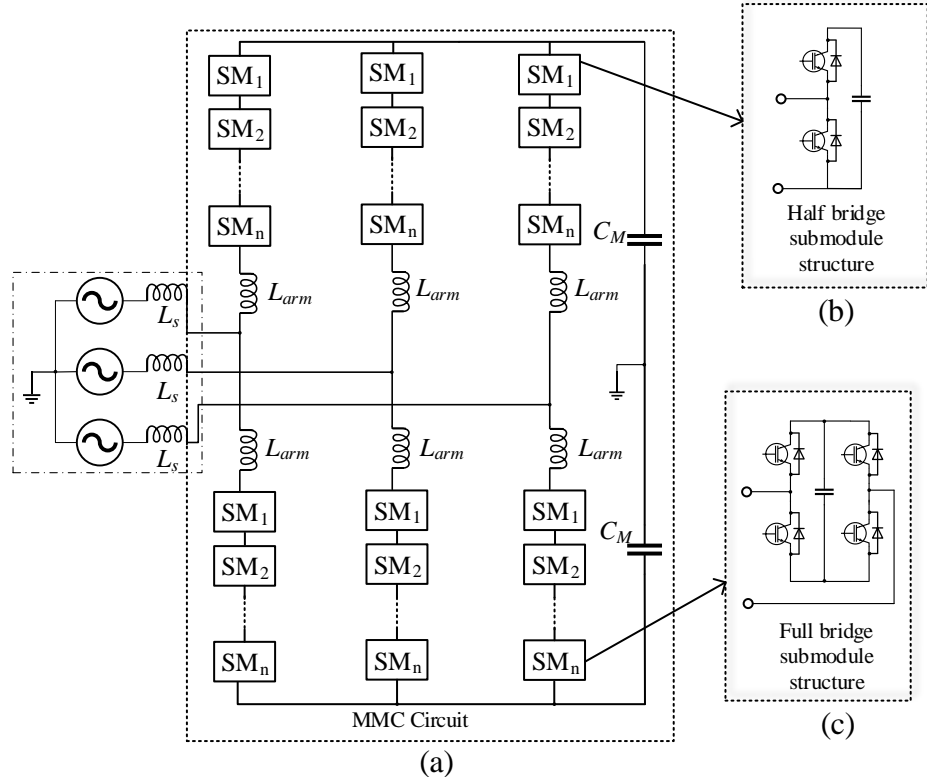


Figure 1.6: (a) MMC circuit (b) Half bridge submodule (c) Full bridge submodule.

Advantage:

- Converter cells are modular and can be easily scaled.
- Any cell of the converter can be easily bypassed during a fault inside it.

- High quality of output is produced so less filter requirement, less power loss, and low dv/dt at output.
- The presence of an arm inductor also helps in limiting short circuit current.
- Excellent transient response during faulty conditions.
- Due to the high voltage rating, the AC side can be directly fed from the grid

Limitation:

- Due to the large no of submodules, the structure of MMC is complex and the cost is higher.
- A large number of big capacitors are required for submodules.
- Control is complex as a large number of PWM signals has to be generated.

1.1.4 What are the advantages of using the NPC-DAB converter?

As previously discussed, DC-DC converters without isolation tend to exhibit higher noise levels, voltage spikes, and transients, compromising system stability and safety. Recognizing the importance of safety and performance, we opted for a Dual Active Bridge (DAB) converter. However, the DAB's low fault tolerance and reduced voltage level posed challenges in achieving the desired outcomes. We turned to the Modular Multilevel Converter (MMC). While effective, the MMC solution proved to be costly and featured complex control mechanisms. To strike a balance between complexity and functionality, we propose the use of a Neutral-Point-Clamped (NPC) DAB converter. This design offers simplicity in both its structure and control mechanisms. Notably, the NPC-DAB has been underutilized in the realm of Electric Vehicle (EV) charging stations. This converter configuration aims to strike a harmonious balance, providing efficient performance while maintaining a manageable level of complexity a crucial consideration in the development of EV charging infrastructure. This converter is thoroughly studied in the literature survey chapter.

Chapter 2

Literature Survey

2.1 Neutral Point Clamped-Dual Active Bridge Converter

Due to its numerous advantages, including high power density, versatile buck and boost conversion capabilities, efficient high-frequency operation, bidirectional power flow, and inherent galvanic isolation, the dual-active-bridge (DAB) has gained widespread application. To enhance the performance characteristics of conventional two-level dual-active-bridge (DAB) converters, we introduce a neutral-point-clamped (NPC) DAB dc-dc converter. The proposed NPC-DAB offers the distinct advantage of being used in high step-up/down converters, particularly in scenarios involving elevated voltages, surpassing the capabilities of conventional two-level DAB systems.

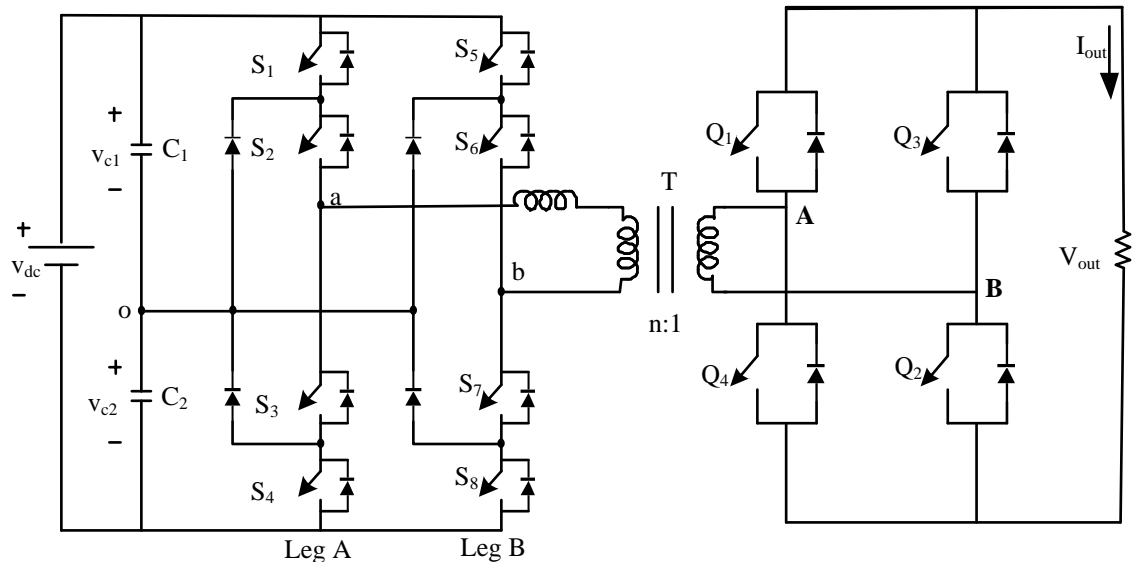


Figure 2.1: 3 level NPC-DAB converter.

2.1.1 Neutral Point Diode Clamped configuration

The neutral point diode clamp (NPC) stands out as a widely embraced and prevalent multi-level topology in medium and high-voltage industrial applications. In this particular NPC dual active bridge configuration, diode-clamped legs (referred to as leg-a and leg-b in the diagram) are utilized to generate a leg-to-leg five-level voltage waveform. The low voltage bridge is manipulated to produce a two-level square waveform across the transformer [10]. In contrast to the two-level voltage source converter, the NPC configuration incorporates clamping diodes that connect the phase output to the neutral point, resulting in a five-level voltage at each NPC leg.

Our analysis focuses on various scenarios of NPC-DAB, assuming a single-phase transformer with unidirectional power flow from the five-level bridge to the two-level bridge. The direction of power flow can be easily controlled by adjusting the phase-shift angle between the active bridges, ensuring a consistent flow from the voltage-leading bridge to the voltage-lagging bridge.

2.1.2 Switching states of the 3L-NPC Bridge

The NPC inverter was initially proposed in 1980 [11]. Subsequently, researchers have actively contributed to various aspects of this converter, delving into topics such as diverse modulation schemes, voltage level variations, capacitor voltage balancing, mitigation of harmonics, and active clamping instead of diodes. In the operational context of NPC-DAB, the switching pattern of the NPC deviates slightly from conventional inverters. Unlike 3L-NPC line frequency inverters (typically at 50 or 60 Hz), where the switching frequency aligns with the line frequency, in NPC-DAB, the switching frequency is equated to the fundamental frequency. To illustrate, Table 2.1 delineates the synthesis of a three-level voltage in a 3L-NPC leg for both positive and negative current flow.

Switching state	Switch S_1	Switch S_2	Switch S_3	Switch S_4	Voltage V_{ao}
+	ON	ON	OFF	OFF	$+V_{DC}/2$
0	OFF	ON	ON	OFF	0
-	OFF	OFF	ON	ON	$-V_{DC}/2$

Table 2.1: Switching State Table.

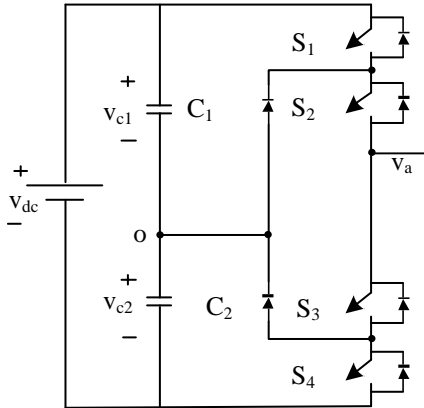


Figure 2.2: Leg A.

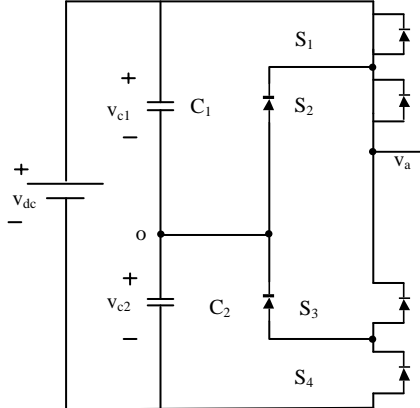


Figure 2.3: "+" switching state.

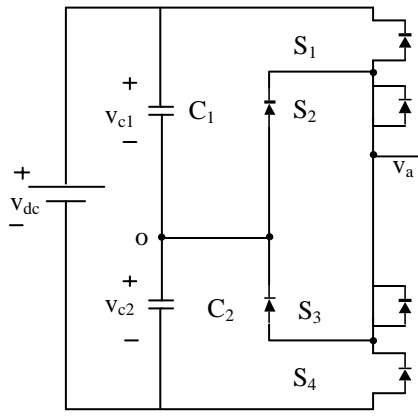


Figure 2.4: "0" switching state.

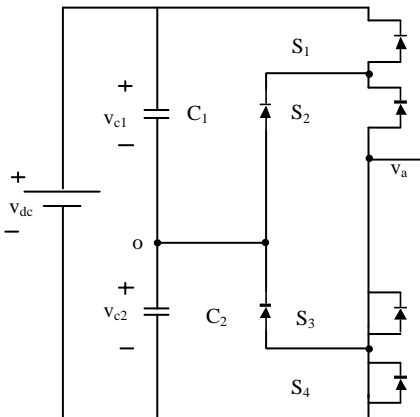


Figure 2.5: "-" switching state.

The figure illustrates key switching states for a three-level (3L) waveform. The primary advantage of the 3L-NPC lies in the fact that, during the commutation between states, all switching devices in a leg endure only half of the DC bus voltage. This characteristic results in lower $\frac{dv}{dt}$ compared to a two-level inverter. It's noteworthy that the switching between the "+" and "-" states is not addressed because of the involvement of all four switches in a leg during this scheme, where two are turned on, and the other two are commutated off [12]. This process, in turn, leads to varying dynamic voltages on each switch, potentially causing double the switching losses. To mitigate this, a small dead time is introduced between different states. The modulation scheme also extends to leg b, where a similar switching pattern is applied to generate a 3L voltage waveform. In this proposed modulation strategy, v_{bo} is phase-shifted from v_{ao} by an amount ($\alpha + \beta$) to generate a voltage waveform (v_{ab}) across the transformer.

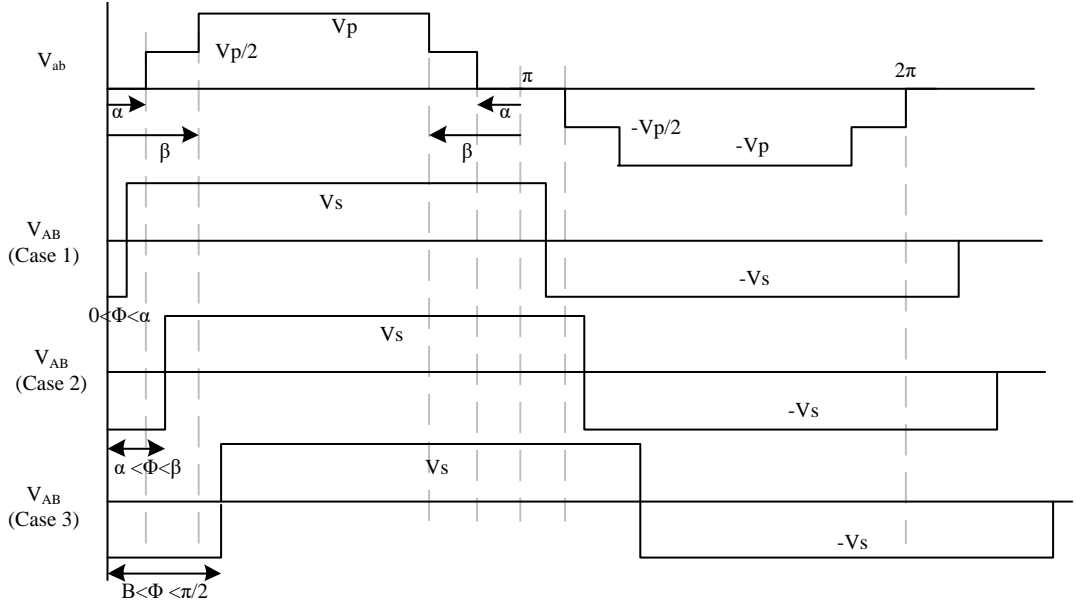


Figure 2.6: Waveform of 5-level NPC-DAB Converter in all three cases.

2.1.3 Power flow equations for 5-level NPC-DAB converter

In NPC-DAB, the management of power flow is governed by the phase-shift angle (ϕ) between v_{ab} and v_{AB} , like the conventional Dual Active Bridge (DAB). Serving as the principal energy transfer element, the leakage inductance of the high-frequency transformer takes centre stage in this process. Represented as L_{LK} in the fig, to delve into the power flow analysis, our focus will be on examining the current i_L coursing through the leakage inductor.

From the basic inductor current

$$v_L = L \frac{di_L}{dt} \quad (2.1)$$

$$Or, i_L = \frac{1}{L} \left[\int_{t_1}^{t_2} v_L dt \right] \quad (2.2)$$

$$Or, i_L = \frac{1}{\omega L} \left[\int_{\theta_1}^{\theta_2} v_L d\theta \right] Where \theta = \omega t \quad (2.3)$$

For $0 < \theta < \phi$

$$i_L(\theta) = \frac{V_s}{\omega L} \theta + i_L(0) \quad (2.4)$$

$$i_L(\phi) = \frac{V_s}{\omega L} \phi + i_L(0) \quad (2.5)$$

For $\phi < \theta < \alpha$

$$i_L(\theta) = -\frac{Vs}{\omega L}\theta + i_L(\phi) \quad (2.6)$$

$$i_L(\alpha) = -\frac{Vs}{\omega L}(\alpha - \phi) + i_L(\phi) \quad (2.7)$$

For $\alpha < \theta < \beta$

$$i_L(\theta) = -\frac{(Vs - \frac{Vp}{2n})}{\omega L}\theta + i_L(\alpha) \quad (2.8)$$

$$i_L(\beta) = -\frac{(Vs - \frac{Vp}{2n})}{\omega L}(\beta - \alpha) + i_L(\alpha) \quad (2.9)$$

For $\beta < \theta < (\pi - \beta)$

$$i_L(\theta) = -\frac{Vp - Vs}{\omega L}\theta + i_L(\beta) \quad (2.10)$$

$$i_L(\pi - \beta) = -\frac{Vp - Vs}{\omega L}(\pi - 2\beta) + i_L(\beta) \quad (2.11)$$

For $(\pi - \beta) < \theta < (\pi - \alpha)$

$$i_L(\theta) = -\frac{(Vs - \frac{Vp}{2n})}{\omega L}\theta + i_L(\pi - \beta) \quad (2.12)$$

$$i_L(\pi - \alpha) = -\frac{(Vs - \frac{Vp}{2n})}{\omega L}(\beta - \alpha) + i_L(\pi - \beta) \quad (2.13)$$

For $(\pi - \alpha) < \theta < (\pi)$

$$i_L(\theta) = -\frac{Vs}{\omega L}\theta + i_L(\pi - \alpha) \quad (2.14)$$

$$i_L(\pi) = -\frac{Vs}{\omega L}(\alpha) + i_L(\pi - \alpha) \quad (2.15)$$

Assuming zero average current through the transformer

$$i_L(0) = -i_L(\pi) \quad (2.16)$$

After solving,

$$i_L(0) = \frac{Vp}{\omega L}\left(\frac{\pi}{2} - \alpha\right) - \frac{Vs}{\omega L}\left(\frac{\pi}{2} - \phi\right) \quad (2.17)$$

Putting this expression of $i_L(0)$ in the above equations, we can get the $i_L(\theta)$ at any point.

The average power flow expression from the primary to secondary bridge through the leakage inductance

$$P_O = \frac{1}{\pi} \left[\int_0^\pi V_{AB}(\theta) \cdot i_L(\theta) d\theta \right] \quad (2.18)$$

After calculating the above power equation using (3), we get the simplified power equation as follows,

Case 1:

$$P_O = \frac{Vp \cdot Vs}{n\omega L} \phi \left(1 - \frac{\alpha}{\pi} - \frac{\beta}{\pi} \right); 0 < \theta \leq \alpha \quad (2.19)$$

Case 2:

$$P_O = \frac{Vp \cdot Vs}{n\omega L} \left(\phi - \frac{\phi^2}{2\pi} - \frac{\alpha^2}{2\pi} - \frac{\phi\beta}{\pi} \right); \alpha < \theta \leq \beta \quad (2.20)$$

Case 3:

$$P_O = \frac{Vp \cdot Vs}{n\omega L} \left(\phi - \frac{\phi^2}{\pi} - \frac{\alpha^2}{2\pi} - \frac{\beta^2}{2\pi} \right); \beta < \theta \leq \frac{\pi}{2} \quad (2.21)$$

2.1.4 Power flow equations for 4-level NPC-DAB converter

In the context of a four-level NPC-DAB (Neutral Point Clamped - Dual Active Bridge) converter, the 0 switching state is not utilized, as referenced in [13]. This has a specific implication for the alpha parameter within the system. In our case, since the 0 switching state is not used, the alpha parameter is set to zero. This essentially means that there is no valid range for the phase shift ϕ where $0 < \phi \leq \alpha$, making case 1 infeasible.

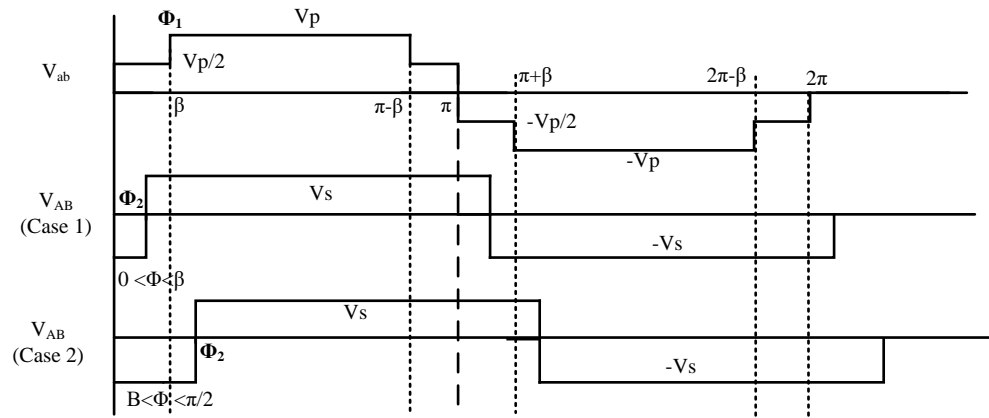


Figure 2.7: Waveform of 4-level NPC-DAB Converter in all three cases.

putting $\alpha = 0$ in all three earlier cases,

Case 1:

$$infeasible, 0 < \phi \leq 0 \quad (2.22)$$

Case 2:

$$P_O = \frac{Vp.Vs}{n\omega L}(\phi - \frac{\phi^2}{2\pi} - \frac{\phi\beta}{\pi}); 0 < \phi \leq \beta \quad (2.23)$$

Case 3:

$$P_O = \frac{Vp.Vs}{n\omega L}(\phi - \frac{\phi^2}{\pi} - \frac{\beta^2}{2\pi}); \beta < \phi \leq \frac{\pi}{2} \quad (2.24)$$

putting $\beta = \phi_1$ and $\phi = \phi_2$

Case 1:

$$\boxed{P_O = \frac{Vp.Vs}{n\omega L}(\phi_2 - \frac{\phi_2^2}{2\pi} - \frac{\phi_1\cdot\phi_2}{\pi}); 0 < \phi_2 \leq \Phi_1} \quad (2.25)$$

Case 2:

$$\boxed{P_O = \frac{Vp.Vs}{n\omega L}(\phi_2 - \frac{\phi_2^2}{\pi} - \frac{\phi_1^2}{2\pi}); \Phi_1 < \phi_2 \leq \frac{\pi}{2}} \quad (2.26)$$

Chapter 3

PCB Design

To build the hardware for the Neutral-Point-Clamped (NPC) converter, the initial step involves the dedicated design and development of a printed circuit board (PCB). This section focuses on the key components and aspects of the NPC hardware setup. The hardware development began with crucial design calculations, including the formulation of a protective circuit on the submodule PCB to address local over and under-voltage concerns. Additionally, the design encompassed the creation of a blanking circuit, a voltage sensing circuit, and the incorporation of a snubber element. Following these calculations, the submodule PCB was designed using Autodesk EAGLE software, detailing the specifics of the various integrated circuit components.

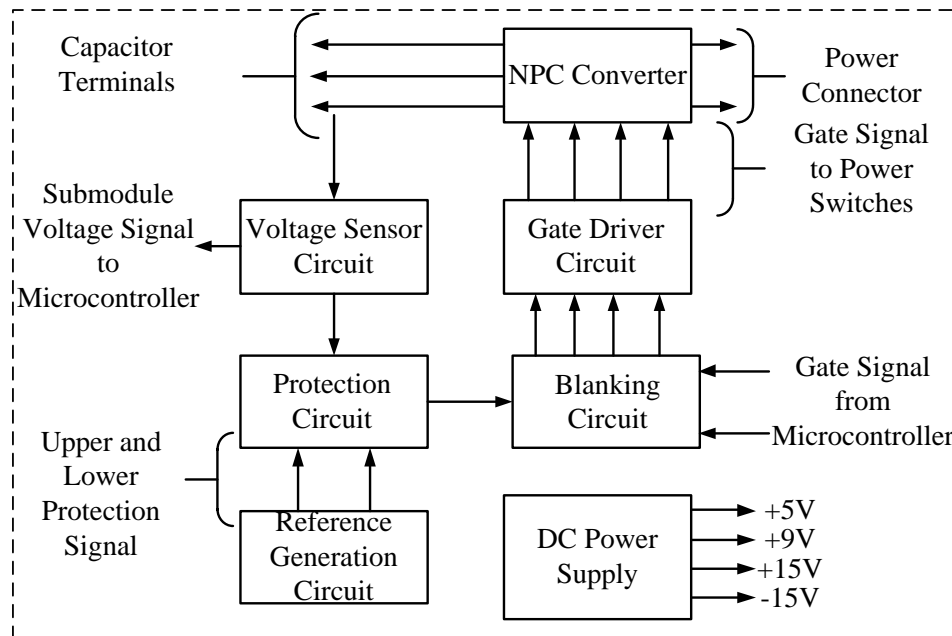


Figure 3.1: Block diagram of modelled PCB.

3.1 Hardware detail of NPC submodule

3.1.1 Power circuit

The power circuit contains four power switches (IGBT FGW75N60HD) which are connected in series. Two fast recovery diodes (STTH25M06FP) are connected in series. The midpoint of the diode and endpoint switch terminals are kept open. Apart from this snubber elements are there in the power circuit which consists of a resistor, capacitor, and diode as the RCD type of snubber is decided for power switches. For snubber, a $2\text{ k}\Omega$ resistor along with a 10 nF capacitor and a fast recovery diode (STTH25M06FP) is used. Fig. 3.2 shows the power circuit schematic of the NPC submodule designed for the implementation of the NPC converter.

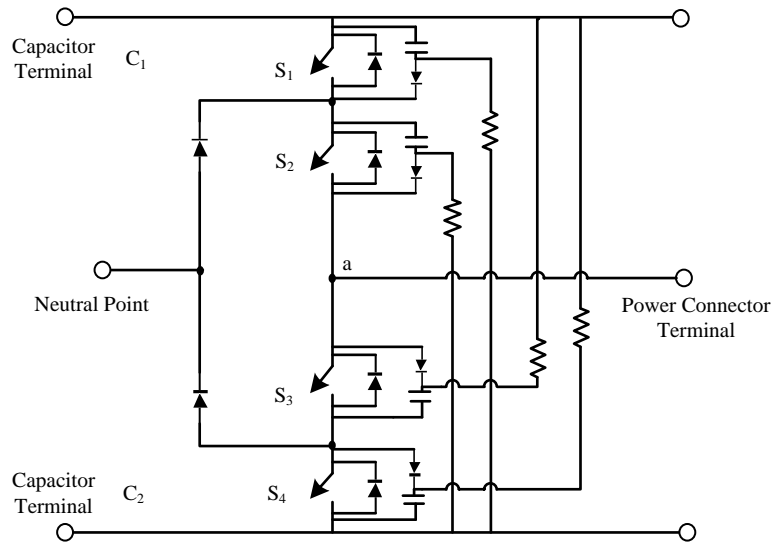


Figure 3.2: Power circuit.

3.1.2 Blanking circuit

The blanking circuit plays a crucial role in introducing a dead time or gap between two gate pulses within the same leg of the system. This dead time is essential to prevent short circuits during transitions, allowing the switches sufficient time to turn off. Selecting an optimal blanking period is critical for ensuring both safety and optimal switch performance. This period is determined based on the operating switching frequency and the

characteristics of the switches. Beyond providing the necessary dead time, the blanking circuit also integrates signals from the protection circuit and the controller. The protection signal offers local protection against over and under-voltage conditions on the submodule, while the block signal provides global protection against various abnormalities related to voltage and current. Figure 3.3 illustrates the schematic of the blanking circuit, employing a re-triggerable monostable multivibrator (74LS123-IC) to generate a dead band between gate pulses within the same leg. This circuit produces a $2.6 \mu\text{ sec}$ blanking period with each rising transition of the pulse. Following the blanking period, the signals are combined with the local protection and block signals, ensuring that activation of any protection signal leads to the blocking of pulses for all switching devices.

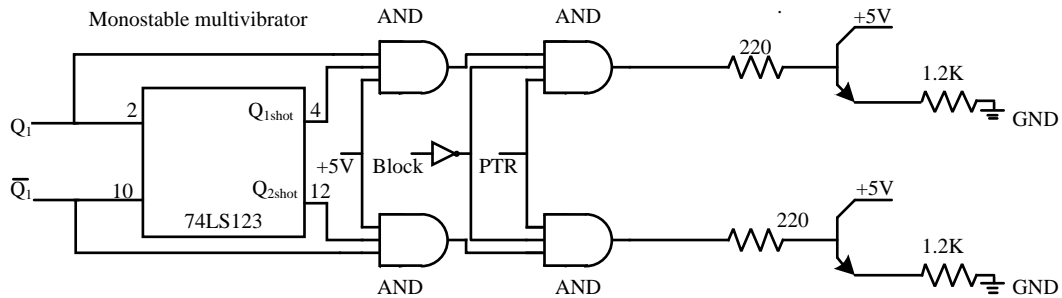


Figure 3.3: Blanking circuit.

3.1.3 Protection circuit

To provide local protection on the submodule PCB, a dedicated circuit has been designed to guard against over and under-voltage conditions affecting the submodule capacitor. In Figure 4.6, the protection circuit schematic for the NPC submodule is shown. The submodule capacitor voltage is sensed through a voltage sensor circuit and compared with predefined limits using a TL064-IC comparator. If these limits are violated, the comparator generates a high signal. This signal passes through a three-input OR gate, undergoes inversion, and acts as a clock pulse for a negative-edge-triggered JK flip-flop (74LS76-IC). Configured with J input set to high and K input set to low, the flip-flop activates the protection signal upon a violation. The design also incorporates fault clearing and protection signal bypass for added flexibility and robustness.

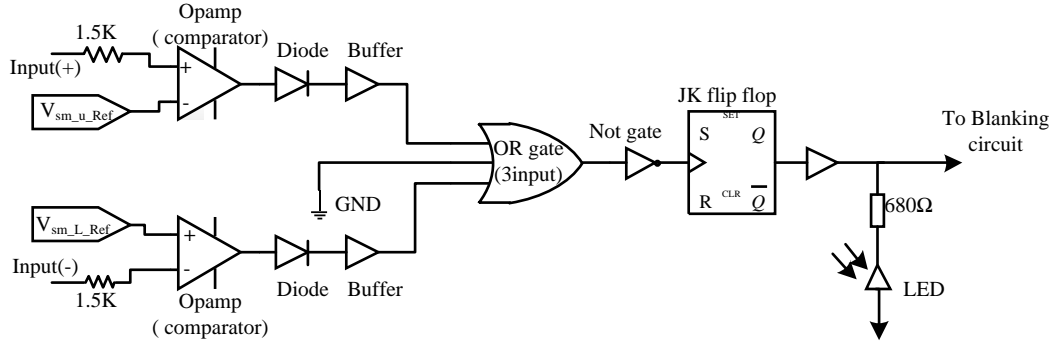


Figure 3.4: Protection circuit.

3.1.4 Gate driver circuit

A Gate driver serves as an interface between the blanking circuit and the gate terminals of the switches, ensuring isolation between the power and control circuits and maintaining appropriate gate pulse levels. The FOD3182 Optocoupler type gate drivers are employed for this purpose, powered by isolated DC-DC converters (MGJ2D151505SC). The pulse from the blanking circuit is transmitted to the driver IC through a buffer. The gate driver is supplied with +15V and -5V. Gate pulses from the gate driver are then connected to the switch gate terminals through a gate resistor (R_G). To regulate the voltage across the gate, two back-to-back Zener diodes are connected across the gate terminal of the switches.

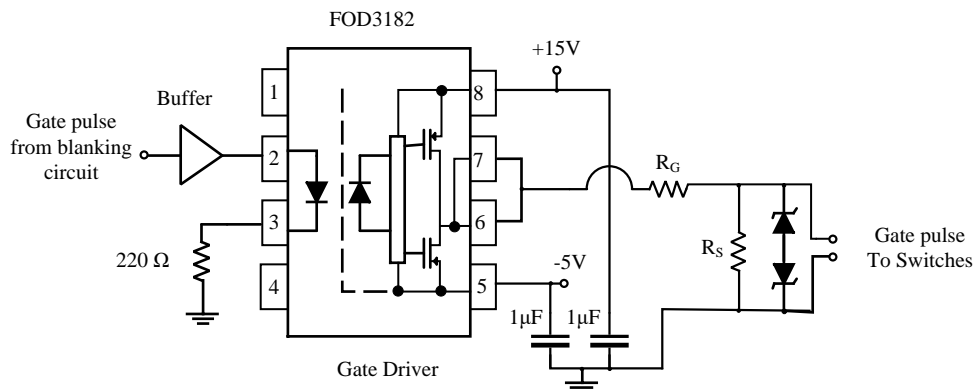


Figure 3.5: Gate driver circuit.

3.1.5 Sensor circuit

A sensor circuit, utilizing LEM LV-25P voltage sensors based on Hall Effect principles, is employed for measuring voltage in the hardware. The LV-25P sensors feature a primary-

to-secondary turn ratio of 2500:1000, adjustable by modifying the resistance value through a trim port resistor. The voltage sensors are precisely tuned at a 1:100 conversion ratio. Figure 3.6 illustrates the schematic circuit diagram of the voltage sensor circuit.

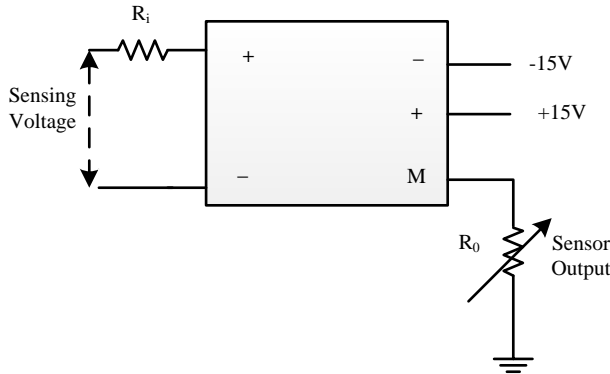
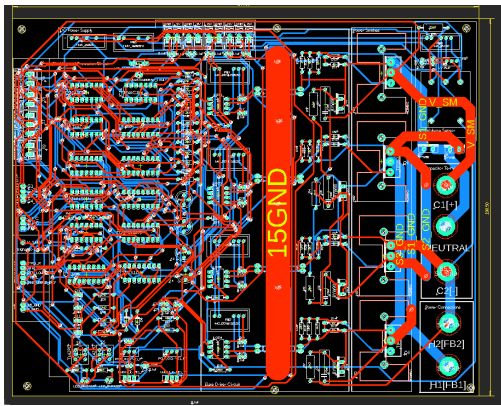


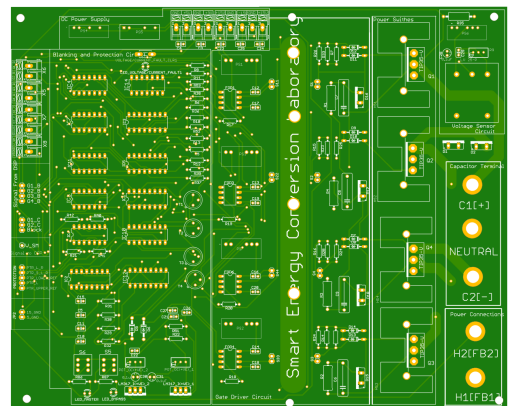
Figure 3.6: Voltage sensor circuit.

3.2 PCB board layout

After creating the schematic using EAGLE, the PCB board layout for the NPC submodule has been meticulously designed, as depicted in Fig-3.7(a). Notably, the power and control circuits are intelligently segregated to minimize interference. The power circuit occupies the right side of the PCB, alongside power connections. To enhance Electromagnetic Interference (EMI) and Electromagnetic Compatibility (EMC) performance, a thick grounded trace is strategically placed on both the top and bottom layers. Control signals traverse from the left side of the PCB, facilitating seamless interchange between signals from and to the controller. The thickness and clearance of traces are meticulously determined based on the current and voltage ratings of the respective traces. DC power supply is introduced from the top of the PCB, with provisions for isolated DC-DC converters strategically placed for different DC supply types. Subsequently, the PCB undergoes fabrication. Fig-3.7(a) illustrates the board layout of the NPC PCB, while Fig-3.7(b) provides a top view of the PCB without components. Fig-3.7(c) illustrates the soldered NPC PCB, while Fig-3.7(d) shows the NPC-DAB converter PCB setup.



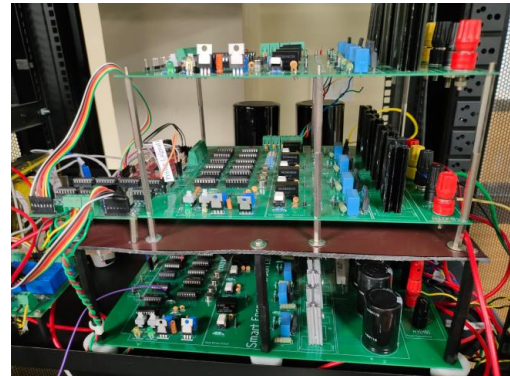
(a) PCB layout.



(b) PCB top view without soldering.



(c) Soldered PCB.



(d) Rack setup.

Figure 3.7: PCB

Chapter 4

Simulation

4.1 Simulation Setup

In this chapter, we will implement both open loop and close loop simulations of the NPC-DAB converter. The configuration starts with two NPC submodules connected at the input side, followed by a series inductor. A transformer is used to connect the primary side to the secondary side. On the output side, an H-bridge submodule is employed.

Figure 4.1 illustrates the schematic model of the NPC-DAB converter used for the simulations.

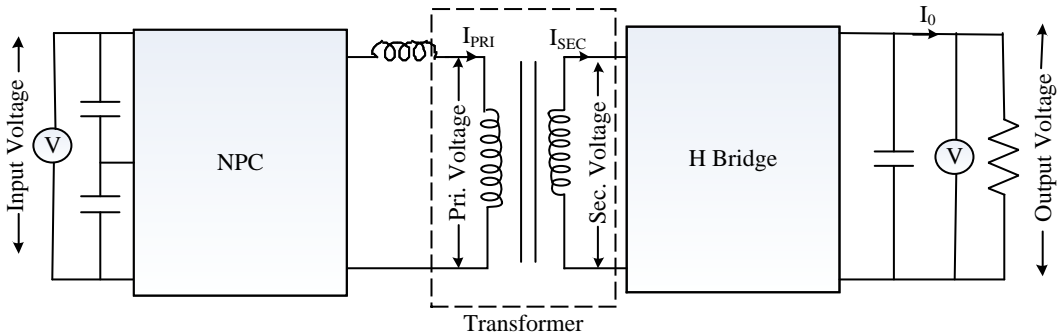


Figure 4.1: NPC-DAB converter.

4.2 Switching Control

In the open loop simulation, we vary the pulse width on the primary side while applying a phase shift on the secondary side.

On the primary side:

- Switch S1 receives a pulse width ranging from $2\phi_1$ to 50%.
- Switch S2 receives a pulse width ranging from 0% to $50\% + 2\phi_1$.
- Switches S5 and S6 receive pulse widths ranging from $50\% + \phi_1$ to ϕ_1 .
- Switches S3, S4, S7, and S8 receive negative pulses corresponding to switches S1, S2, S5, and S6, respectively.

On the secondary side:

- Switches are given a 50% pulse width, phase-shifted by $\phi_1 + \phi_2$.

This configuration ensures proper timing and coordination of the switching pulses, facilitating the desired operation of the NPC-DAB converter. The switching pulse waveforms are shown in the following figure.

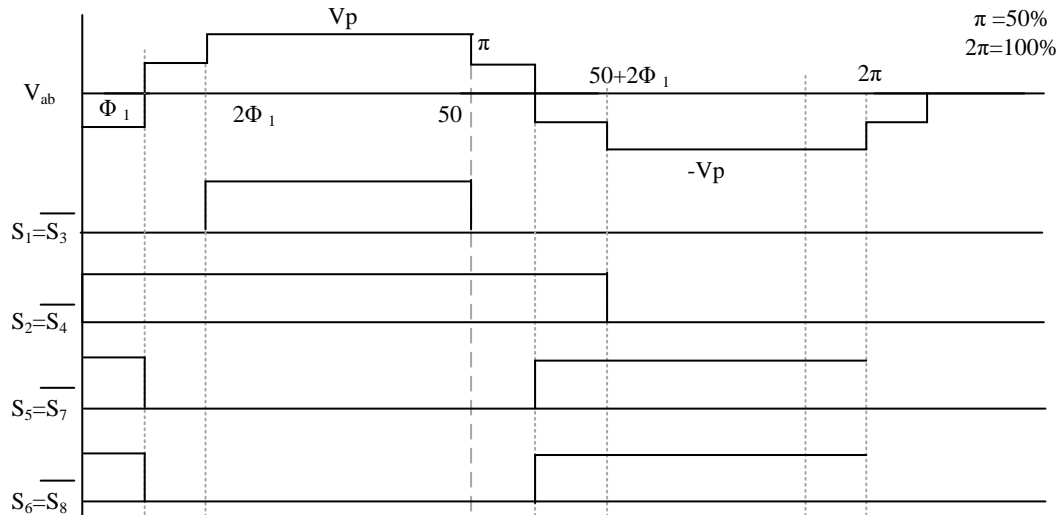
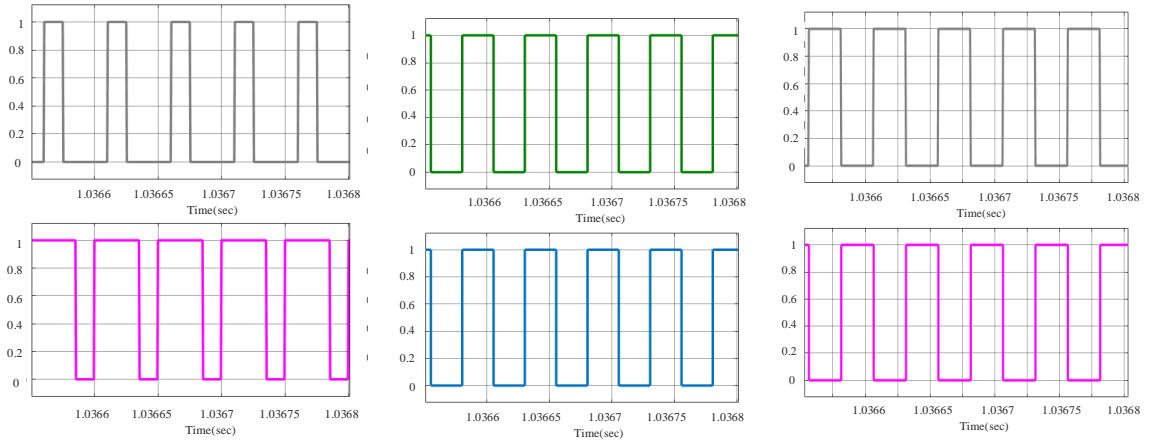


Figure 4.2: Switching technique for NPC-DAB converter.

4.3 Open loop control of NPC-DAB converter

This setup involves two 100V input supplies (200V total) in an open loop configuration, which are modulated at a frequency of 20 kHz. The primary side inductance is set to $65\mu H$, ensuring the inductive reactance at the switching frequency is appropriate for the



(a) Switching pulse of switch S_1, S_2 . (b) Switching pulse of switch S_5, S_6 . (c) Switching pulse of switch Q_1, Q_2 .

Figure 4.3: Switching pulses for different switches.

converter's operation. The nominal power transfer rating of 18 kVA specifies the maximum power that can be effectively transferred under nominal operating conditions. The various other parameters crucial for the simulation are provided in the table. Figures 4.4 and 4.5 depict the simulation diagram and the control scheme for the NPC-DAB converter.

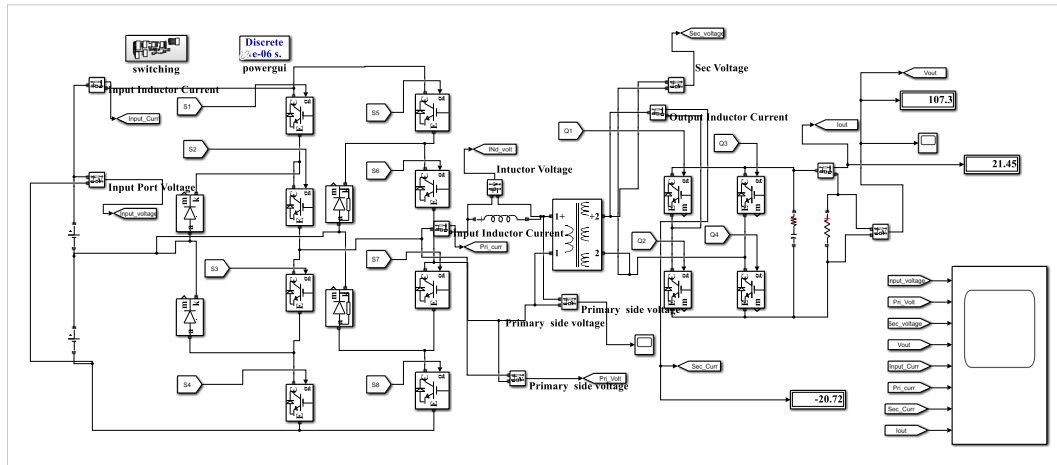


Figure 4.4: Open loop simulation of 3-level NPC-DAB converter.

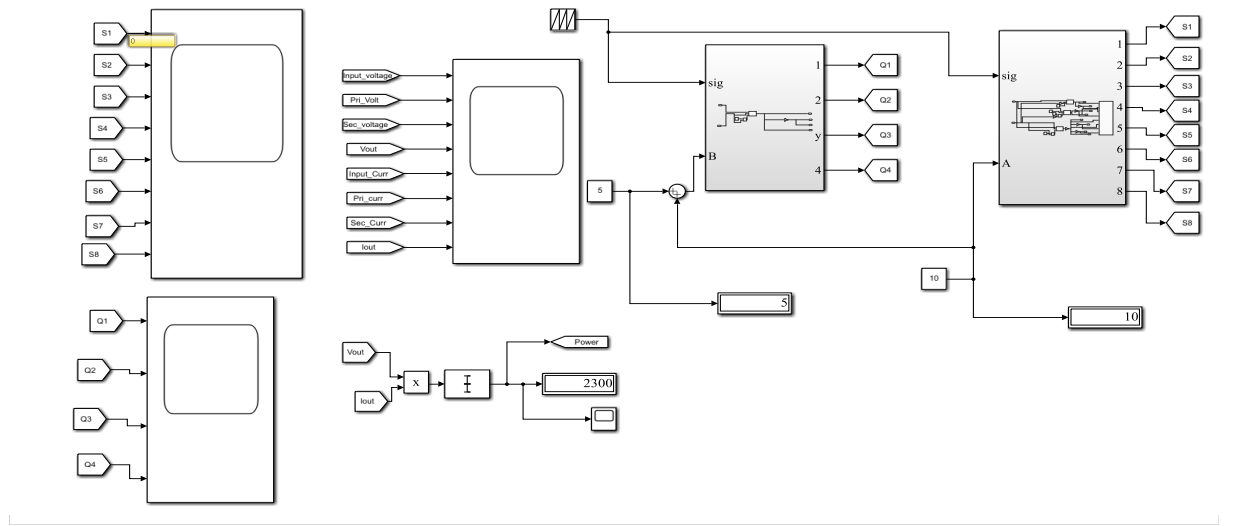


Figure 4.5: Switching control subsystem.

Simulation Specification	Value
DC input voltage	200
Converter rating	18 kVA
Arm inductance	$65 \mu\text{H}$
Winding leakage inductance	$130 \mu\text{H}$
Winding nominal voltages [U1 U2] (Vrms)	200V, 100V
Output capacitor	$1000 \mu\text{F}$
Switching frequency	20 kHz
Load	5Ω

Table 4.1: Simulation parameters for open loop operation of NPC-DAB converter.

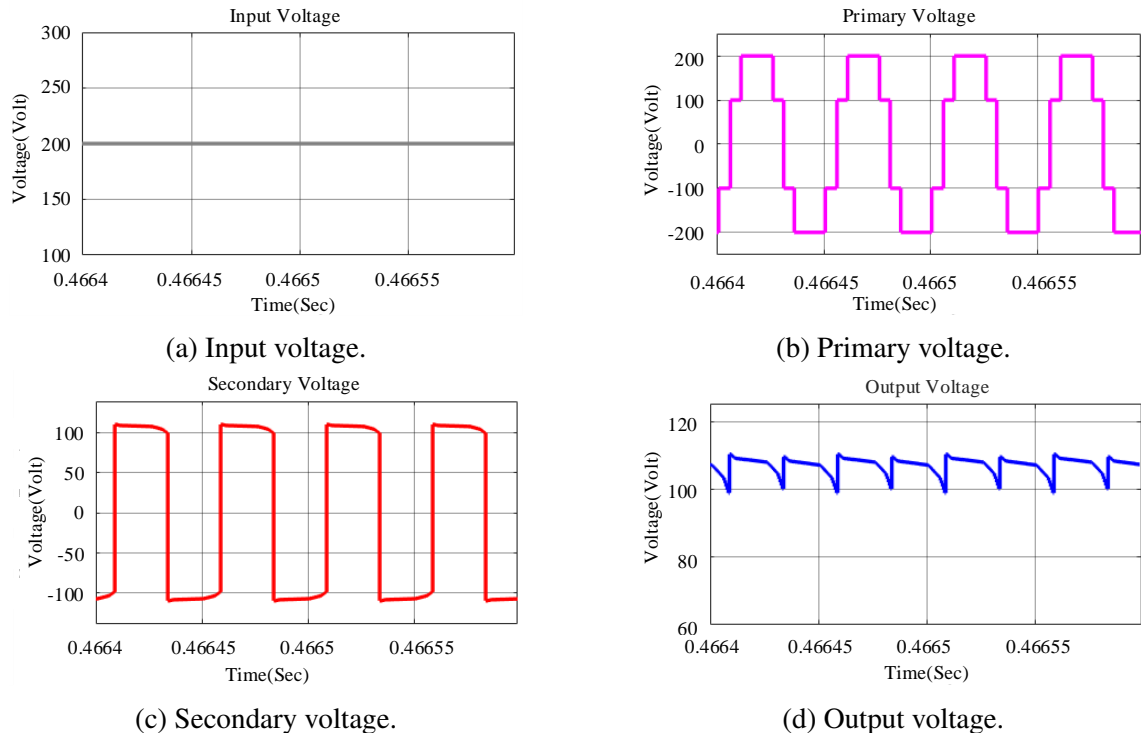


Figure 4.6: Voltage waveforms in open loop simulation for load $R = 5\Omega$. Simulation 26

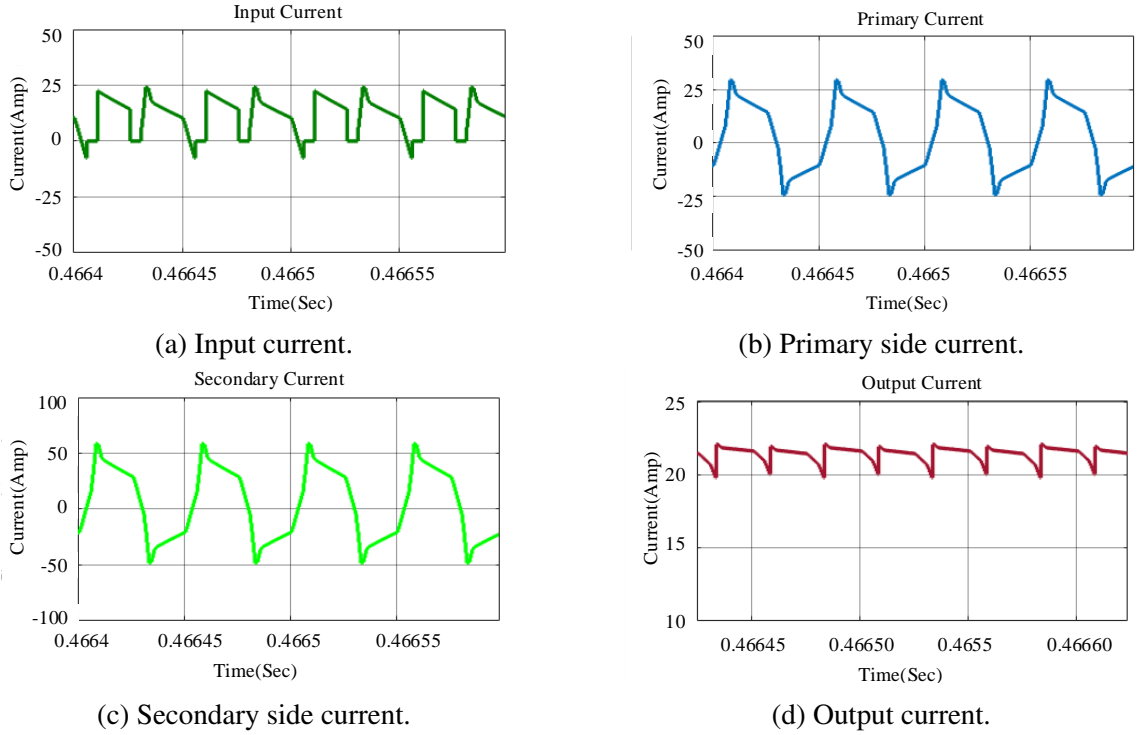


Figure 4.7: Current waveforms in open loop simulation for load $R = 5\Omega$.

As per our theoretical analysis, the primary voltage waveform comprises 4 levels ($V_{DC}, \frac{V_{DC}}{2}, -\frac{V_{DC}}{2}, -V_{DC}$), while the output port voltage waveform exhibits 2 levels ($V_S, -V_S$). Remarkably, our simulation faithfully reproduces the expected waveforms, with the input port voltage evolving through 4 distinct steps and the output port voltage maintaining the theorized 2-level pattern.

4.4 Close loop control of NPC-DAB converter

Close loop control, also known as feedback control, is essential in various applications to maintain the desired system output by automatically adjusting its inputs. Therefore, to control the output voltage of an NPC-DAB converter, a close loop simulation is required. In this close loop operation, the reference voltage can be adjusted at any moment to achieve the desired output voltage.

In contrast, in open loop control, the output voltage is fixed to the reference value and any change in the load will cause the output voltage to fluctuate. To address this issue, we are using a single-phase shift technique. This technique helps to regulate the output voltage by

dynamically adjusting the phase shift based on feedback from the system, ensuring stable and accurate voltage control even with varying loads.

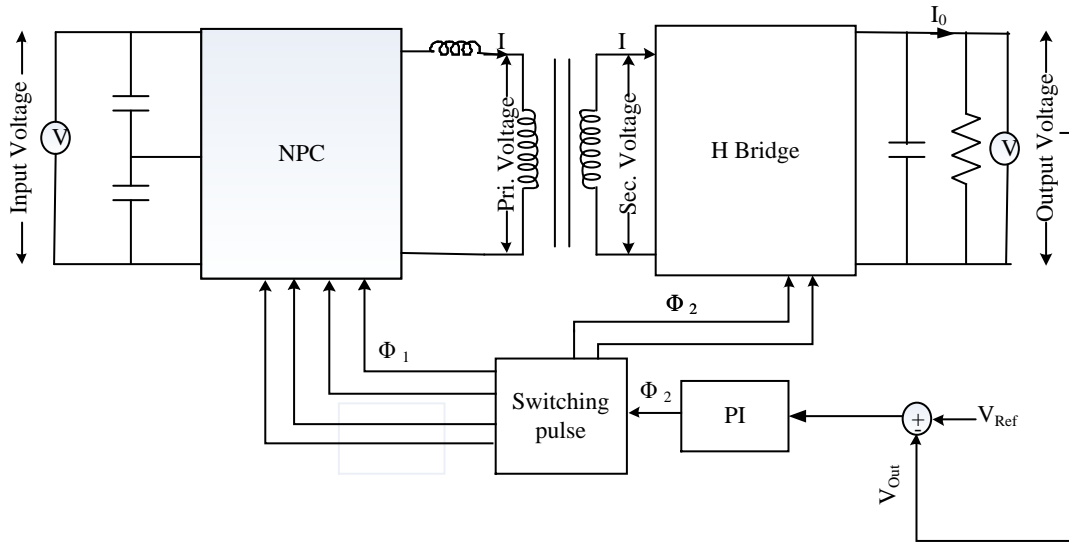


Figure 4.8: Close loop scheme for NPC-DAB converter.

In a close loop simulation, we are using a single-phase shift technique to regulate the output voltage. figure 4.8 illustrates the close loop control scheme for NPC-DAB converter. Here is a step-by-step explanation of the process:

1. **Comparison of Voltages:** The output voltage is compared with a reference voltage. This comparison generates an error signal, which represents the difference between the actual output voltage and the desired reference voltage.
2. **PI Controller:** The error signal is passed through a Proportional-Integral (PI) controller. The PI controller is designed to reduce the error over time and bring the output voltage closer to the reference voltage. In our simulation, the proportional gain (P) is set to 1, and the integral gain (I) is set to 10. These values were determined using a hit-and-trial method, aiming to achieve optimal performance.
3. **Second Phase Shift:** Finally, the output of the PI controller is sent to the second phase shift component. This component further processes the signal to achieve the desired phase shift in the system, contributing to the overall regulation of the output voltage.

By following these steps, the close loop system aims to maintain the output voltage at the

desired level by continuously adjusting based on the feedback from the system. Our close loop simulation investigated the system's response under different load conditions:

4.4.1 At $R=20\Omega$

In this simulation, we are using two 100-volt input sources. ϕ_1 is 15 percent. The inductance value is $65 \mu H$, and the load resistance is 20Ω . The transformer turn ratio is 200V/100V, and the reference output voltage is set to 100V.

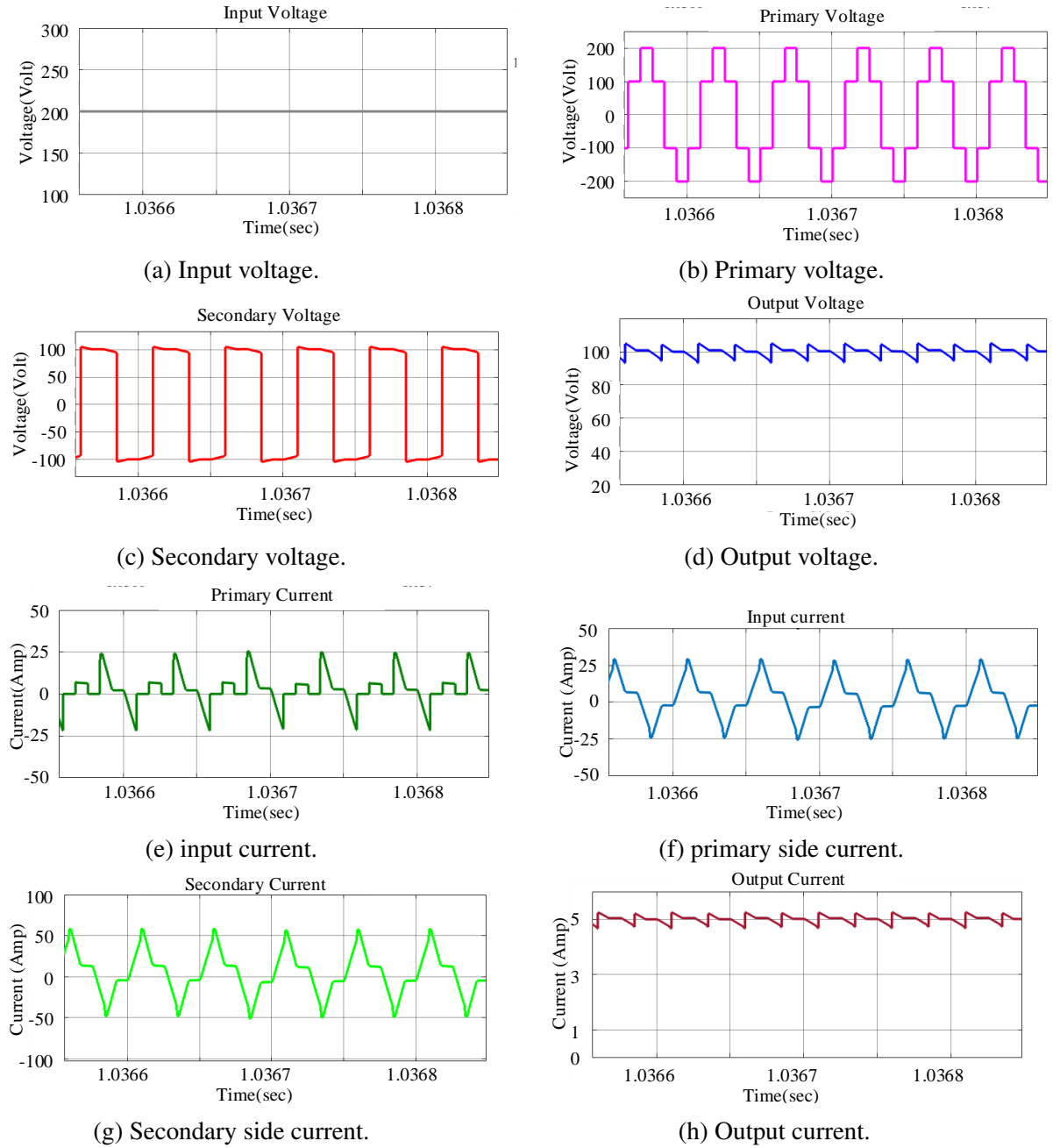


Figure 4.9: Waveforms for $R = 20\Omega$.

4.4.2 At $R=10\Omega$

In this simulation, we are using two 100-volt input sources. ϕ_1 is 15 percent. The inductance value is $65 \mu H$, and the load resistance is 10Ω . The transformer turn ratio is 200V/100V, and the reference output voltage is set to 100V.

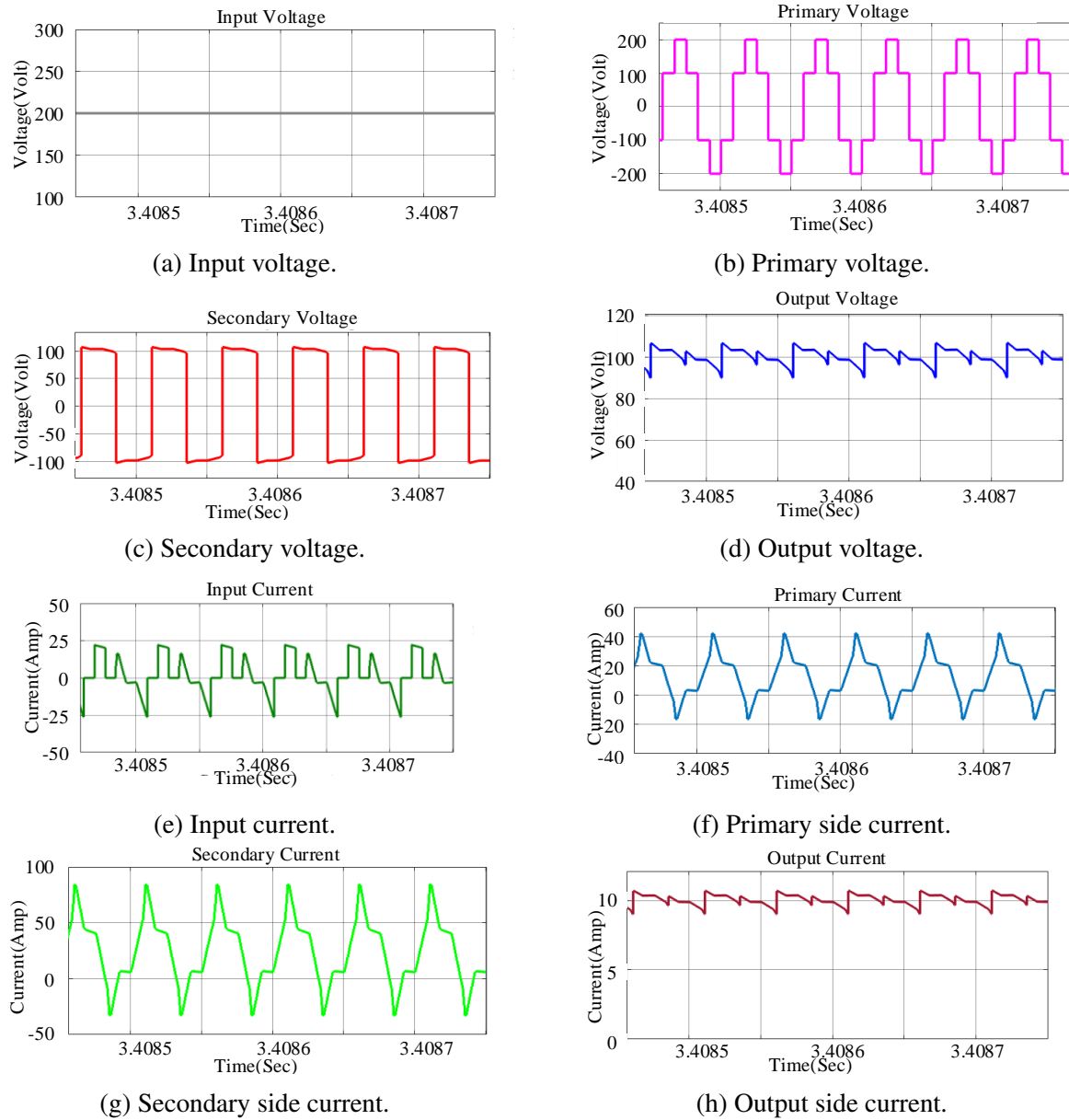


Figure 4.10: Waveforms for $R = 10\Omega$.

4.4.3 When R change from 20Ω to 10Ω

In this simulation, we investigate the system's response to a step change in load from 20Ω to 10Ω at $t = 2$ seconds. All parameters remain identical to the previous setup.

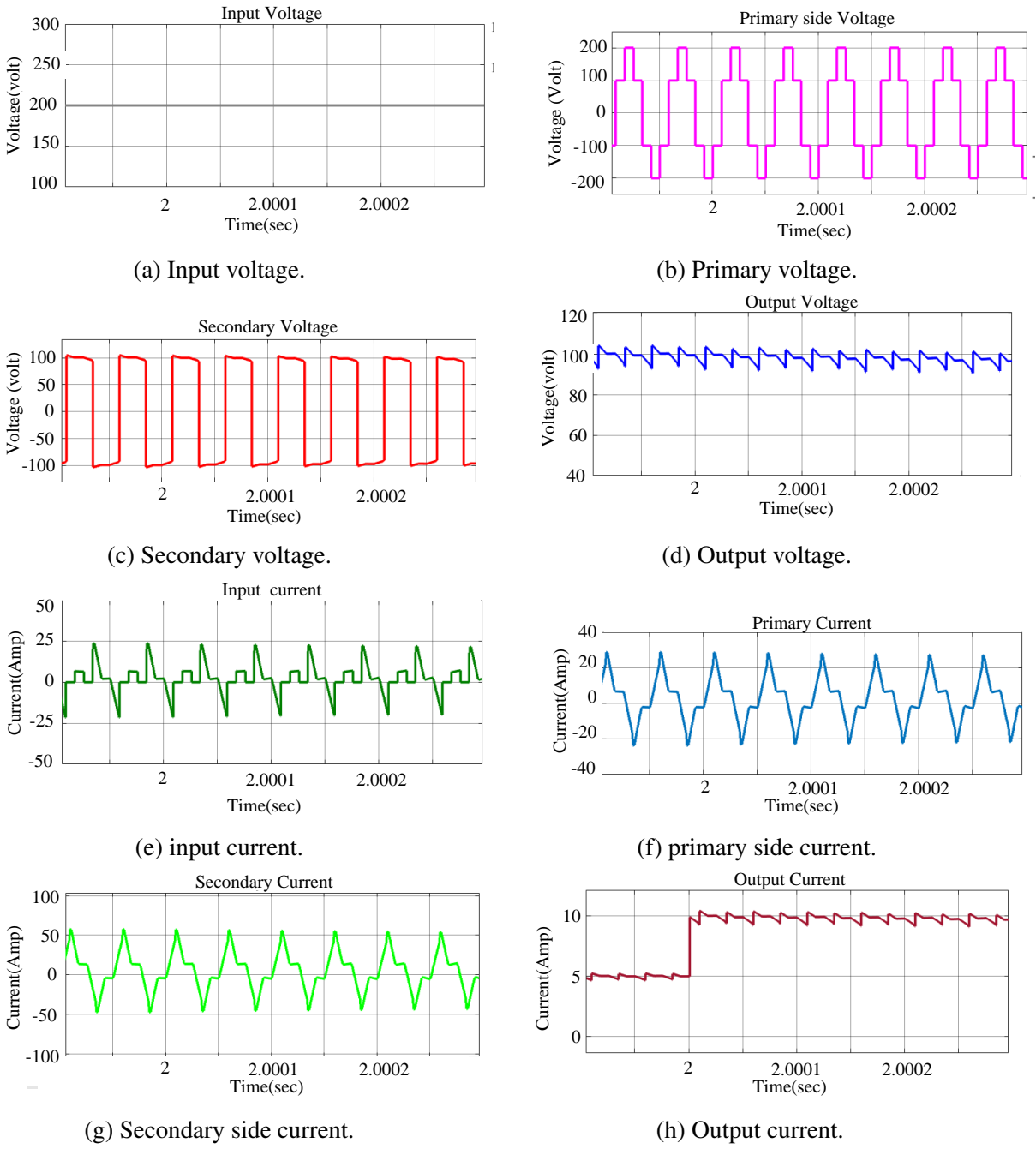


Figure 4.11: Waveforms for $R = 20 \Omega$ to $R = 10 \Omega$.

The simulation results demonstrate that the output voltage remains constant despite the load change from 20Ω to 10Ω at $t = 2$ seconds. Conversely, the output current increases from 5 A to 10 A at the same time point. This behaviour confirms the successful close loop operation of the converter, as it maintains a regulated output voltage even under varying load conditions.

Chapter 5

Hardware Setup and Result

5.1 Hardware Setup

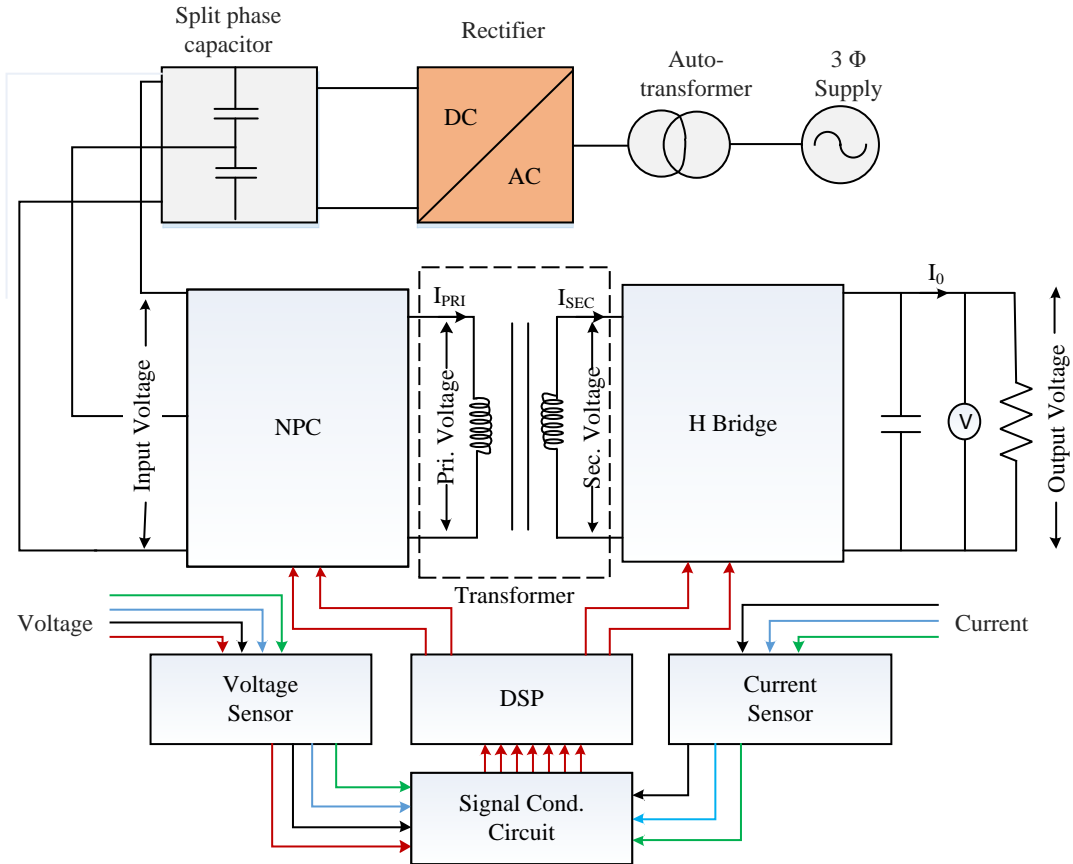


Figure 5.1: Hardware schematic.

Figure 5.1 illustrates the schematic diagram of our hardware setup. The system starts with a three-phase supply that is fed into an auto-transformer. The output from the auto-transformer is directed to a rectifier, which converts the AC input to DC. This DC output

is then delivered to a split-phase capacitor, which divides the DC supply into two equal halves, creating two equal half-voltage supplies.

These half-voltage supplies are subsequently fed into the NPC-DAB converter. The switching operations of the converter are controlled by a DSP, which is operated by a host computer.

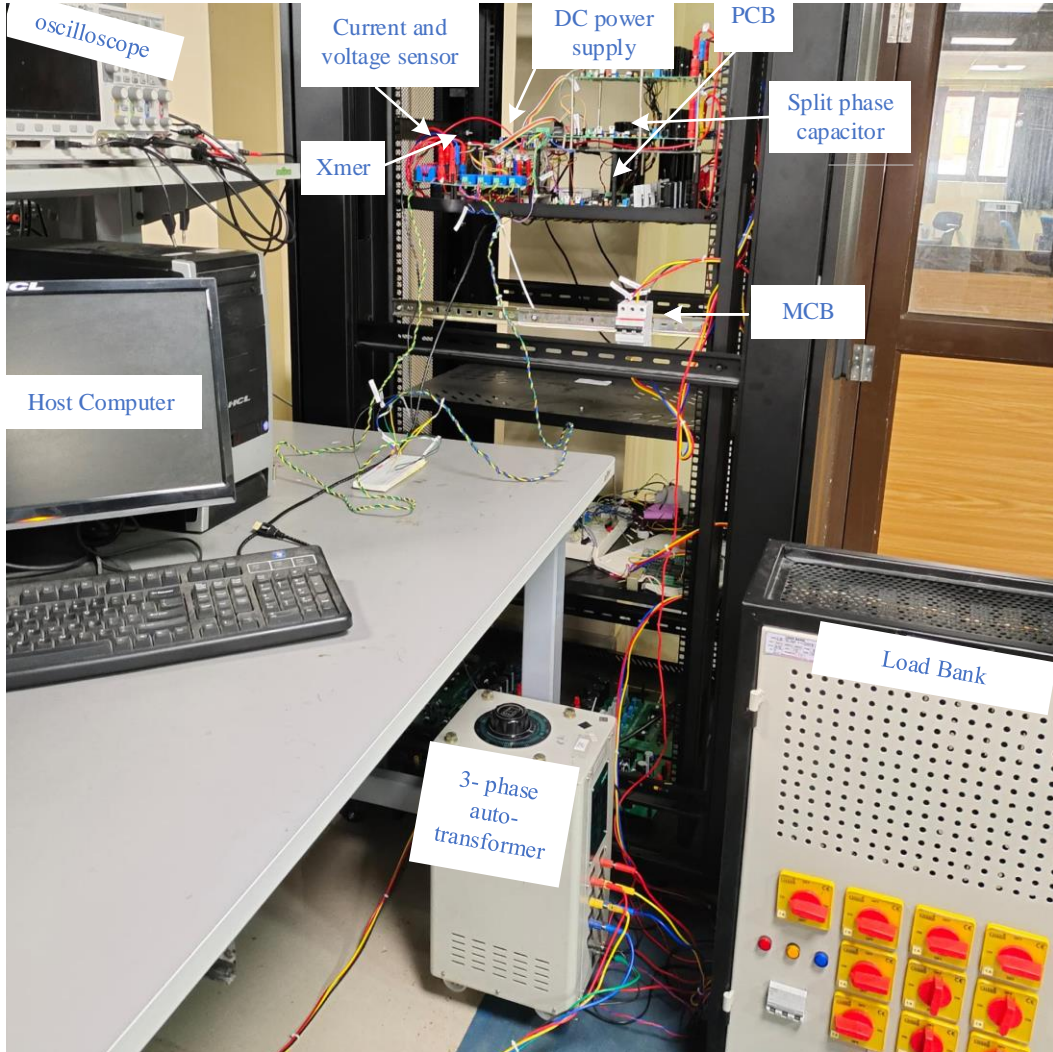


Figure 5.2: Full rack setup.

Figure 5.2 illustrates the complete rack setup of our NPC-DAB hardware configuration, while Figure 5.3 shows the PCB rack setup. Figures 5.4 to 5.9 highlight the individual components, including the NPC sub-module, H-bridge sub-module, voltage and current sensors, DSP, transformer, and others. These circuits are explained in detail below.

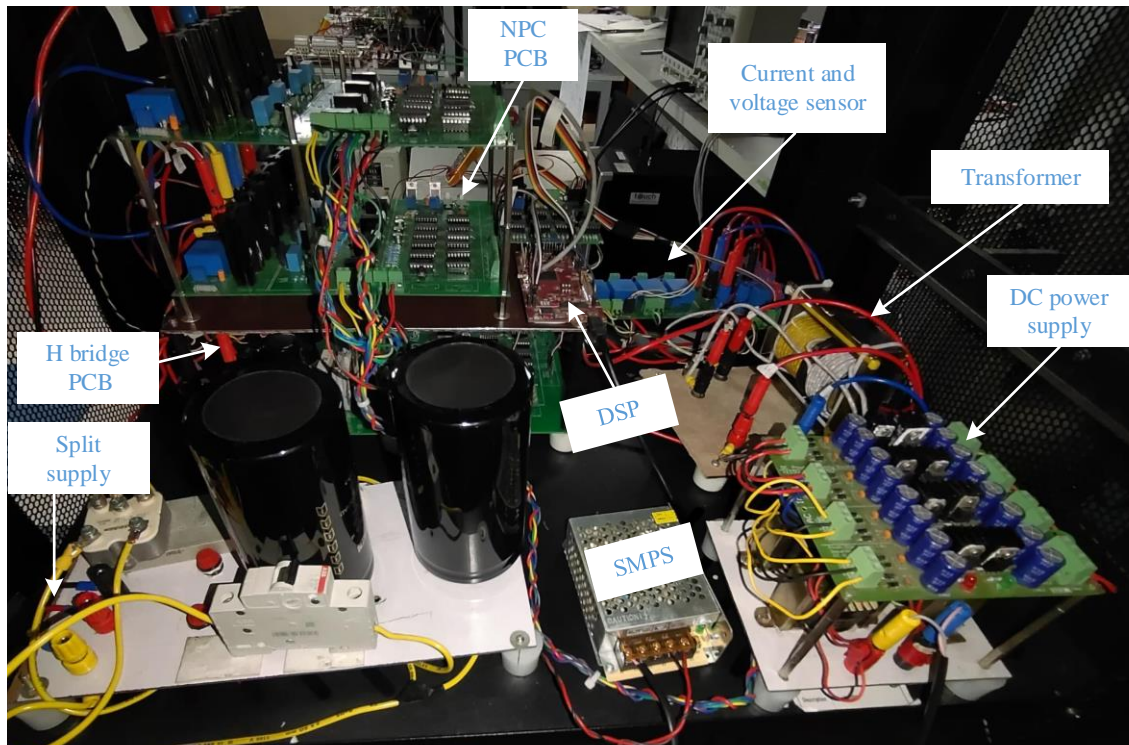


Figure 5.3: Rack PCB setup.



Figure 5.4: Picture of NPC submodule.

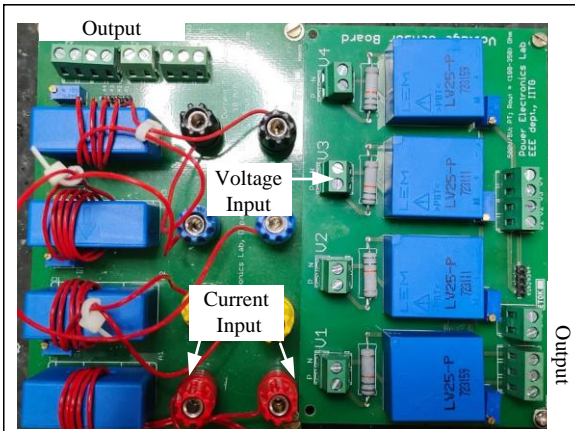


Figure 5.5: Picture of Sensors.



Figure 5.6: Picture of H Bridge PCB.

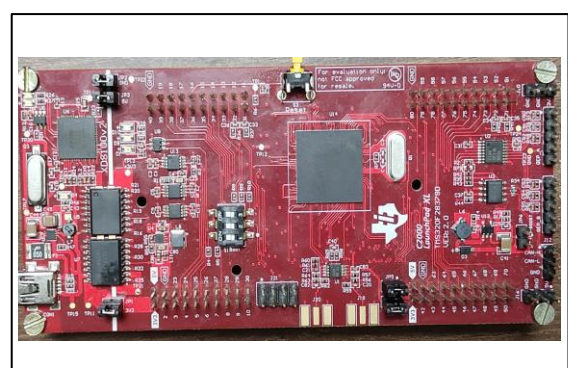


Figure 5.7: Picture of DSP.

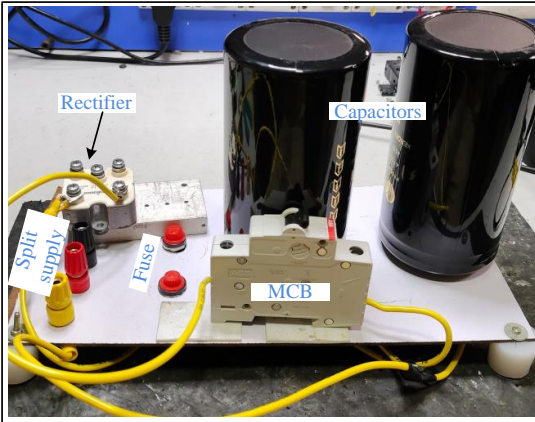


Figure 5.8: Picture of Split DC Supply.

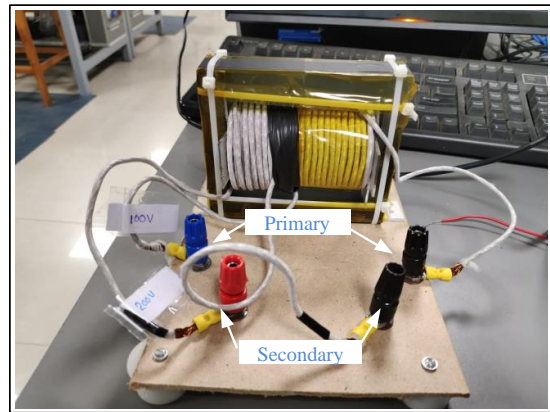


Figure 5.9: Picture of Transformer.

5.1.1 NPC submodule

The NPC submodule integrates not only the power circuit but also crucial circuit like protection circuits, gate drivers, and blanking circuits. The design emphasizes the intelligent segregation of power and control circuits to minimize interference. On the PCB, the power circuit is positioned on the right side alongside the power connections. To enhance Electromagnetic Compatibility (EMC) and mitigate Electromagnetic Interference (EMI), thick grounded traces are strategically placed on both the top and bottom layers.

Control signals efficiently traverse from the left side of the PCB, facilitating seamless communication between the controller and other components. Trace thickness and clearance are meticulously optimized based on the current and voltage ratings to ensure reliable operation. DC power is supplied from the top of the PCB, with isolated DC-DC converters strategically located to accommodate different DC supply requirements. Figure 5.4 illustrates the NPC PCB submodule.

5.1.2 H Bridge Submodule

The H-bridge submodule consists of two legs, each containing two switches that operate in a complementary fashion. This PCB also includes protection circuits, gate driver circuits, and blanking circuits. Control signals traverse efficiently from the left side of the PCB, ensuring seamless communication between the controller and other components. Trace thickness and clearance are carefully optimized based on current and voltage rat-

ings to guarantee reliable operation. DC power is introduced at the top of the PCB, with isolated DC-DC converters strategically positioned to accommodate various DC supply requirements. Figure 5.5 depicts the MMC submodule.

5.1.3 Transformer

Designing a transformer involves a series of critical steps, including defining specifications, selecting the core material, calculating winding parameters, and ensuring thermal and insulation requirements are met [14]. Figure 5.6 illustrates the designed transformer. Below is a detailed step-by-step guide:

Define Specifications: For our operation our input (primary) and output (secondary) voltages are 400V and 200V respectively. The operating frequency is 20 KHz.

Core Selection: For our operation we selected a ferrite core whose specifications are the following

For ferrite core E 100/60/28

$$Bm = 0.2T$$

$$Ae = 735 \text{ mm}^2$$

$$f = 20KHz$$

Winding Calculations; As we Know $[E=4.4fN\Phi_m]$

Where, $\Phi_m = Bm * Ae$. Then

$$N = \frac{E}{4.4 * f * Bm * Ae}$$

$$N = \frac{400}{4.4 * 2 * 10^4 * 735 * 10^{-6} * 0.2}$$

$$N = 30.9 \approx 32$$

$$N2 = 16$$

5.1.4 DSP

The LAUNCHXL-F28379D serves as an affordable tool for evaluating and developing TMS320F2837xD products in the TI MCU LaunchPad™ development kit ecosystem [15]. We are actively simulating DSP algorithms through MATLAB/Simulink. Though this traditional approach is suitable for offline DSP algorithm practice, it also enhances online application performance, offering insights beyond what MATLAB/Simulink simulations alone can provide.

In MATLAB/Simulink, we create code for switching pulses, protection circuits, and closed-loop control systems. Specifically, for the switching pulses, switch S_1 is assigned a pulse width between $2\phi_1$ and 50% while switching S_2 receives a pulse width from 0 to $50\% + 2\phi_1$. Similarly, switches S_5 and S_6 are given pulse widths from 0 to 50%. For the secondary side, switches Q_1 and Q_2 have pulse widths ranging from $\phi_1 + \phi_2$ to $50\% + \phi_1 + \phi_2$.

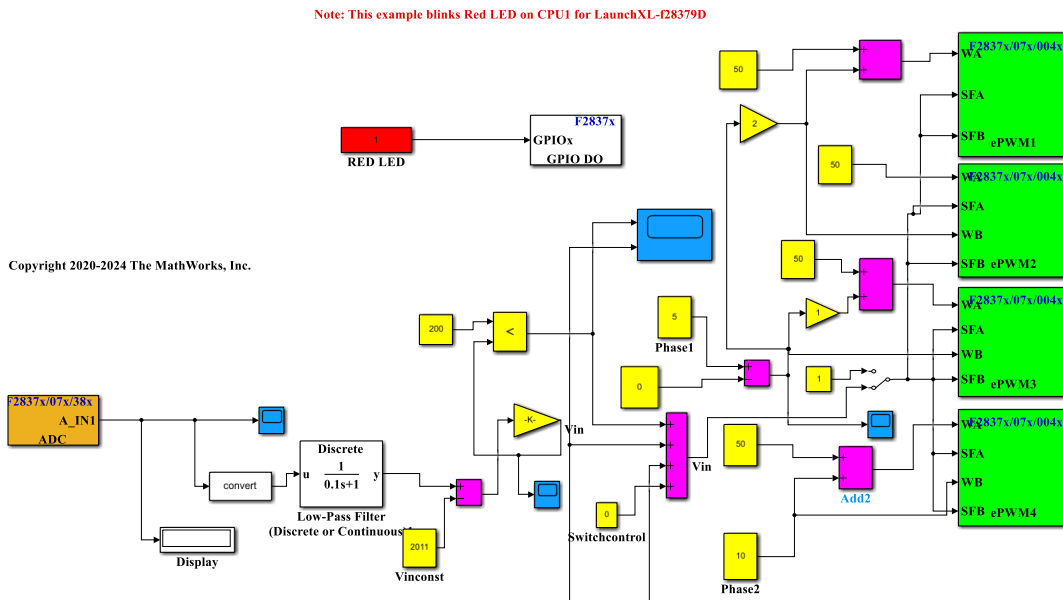


Figure 5.10: DSP switching pulse and protection

Online protection: For protection, we acquire V_{in} , V_{pri} , V_{sec} , V_{out} , I_{pri} , I_{sec} , I_{out} from current transformers (CTs) and potential transformers (PTs) output. All the scaled-down values are first passed through a low-pass filter. Then, the voltages are scaled up by a factor of 100, and the currents are scaled up by a factor of 2. These values are compared

with predetermined upper voltage and current limits. If any of the values exceed these limits, a signal is generated to stop the switching pulses, thereby protecting the circuit.

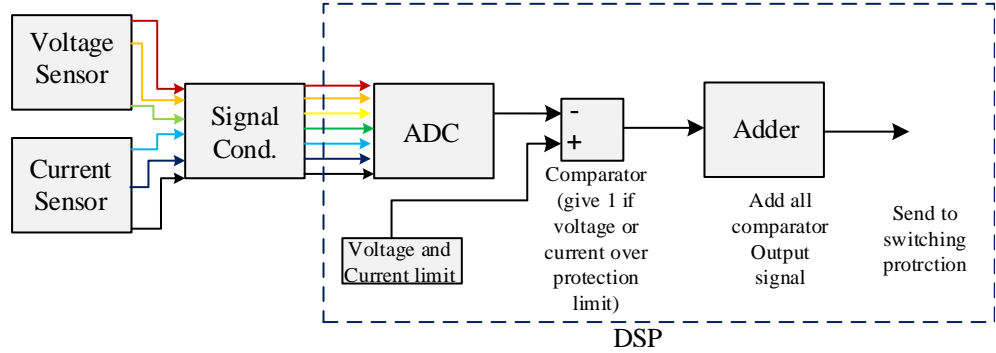


Figure 5.11: DSP protection

5.2 Open loop control of NPC-DAB converter

NPC-DAB hardware testing is started with open loop operation. The switching method is simulated using Simulink, and a .hex model is produced for Digital Signal Processor (DSP). Every submodule has local protection mechanisms that have been engaged in addition to a global protection system that is part of the DSP. To provide +15 V, +12 V, +9 V, and +5 V to integrated circuits (ICs), a separate DC voltage supply is utilized. Continuous measurements of voltage and current are made, with results scaled down to represent actual magnitudes by factors of 20 for current and 1000 for voltage. These readings are checked against preset fault criteria at each instant. Any voltage or current that exceeds these thresholds causes a signal to be activated. Figure 5.12, 5.13 illustrates the switching pulse for the open-loop condition.

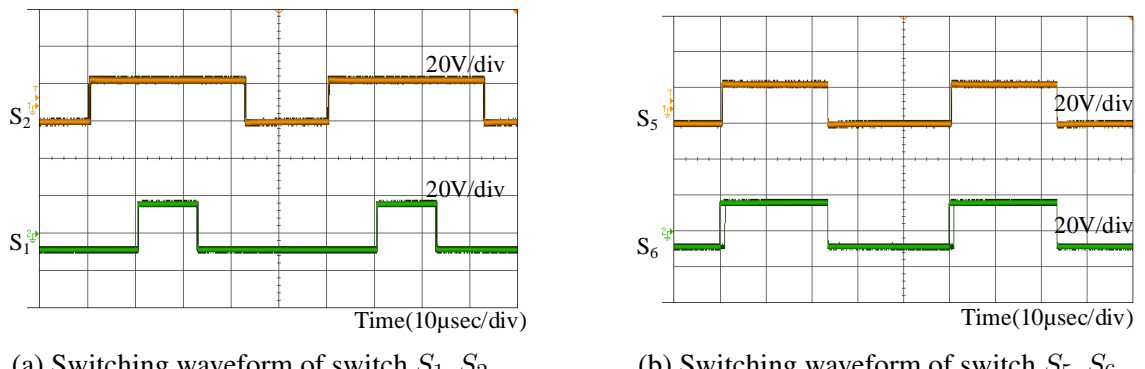


Figure 5.12: Waveforms for different switches and conditions

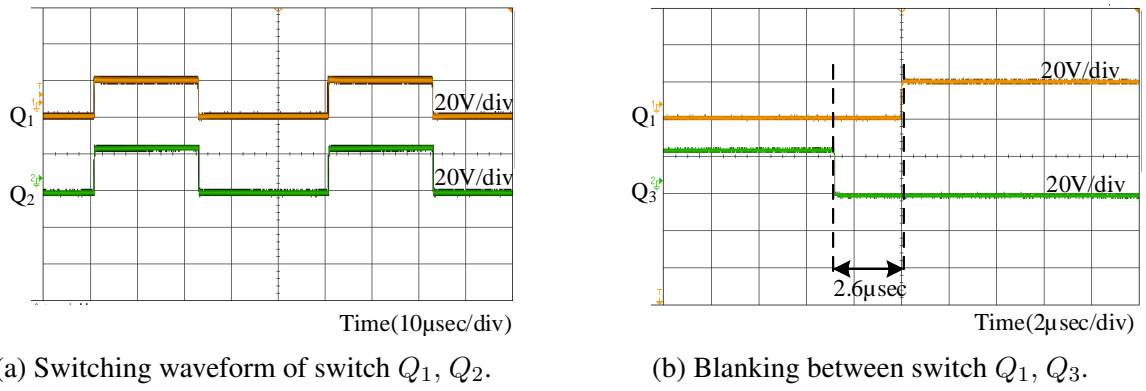


Figure 5.13: Waveforms for different switches and conditions

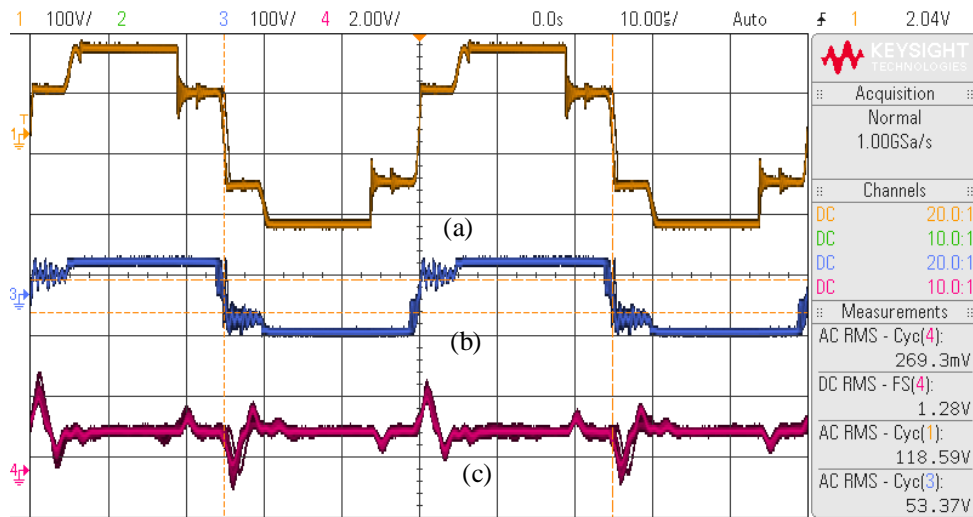


Figure 5.14: (a) Primary side voltage, (b) Secondary side voltage, (c) output current

Figure 5.14 depicts the voltage waveforms of both the primary and secondary sides of the NPC-DAB. The input DC voltage is set at 150V. The phase shift ϕ_1 is 10%, equivalent to 36 degrees, while ϕ_2 is 1%, equivalent to 3.6 degrees. Voltage and current waveforms are observed on the DSO (Digital Storage Oscilloscope). Since two NPC submodules are used on the primary side of the NPC-DAB, four distinct levels are clearly visible in the output waveform.

5.3 Close Loop control of NPC-DAB converter

To run the hardware in a closed-loop configuration, we need components such as a voltage sensor, a signal conditioning circuit, and a DSP. Figure 5.15 illustrates the connection scheme.

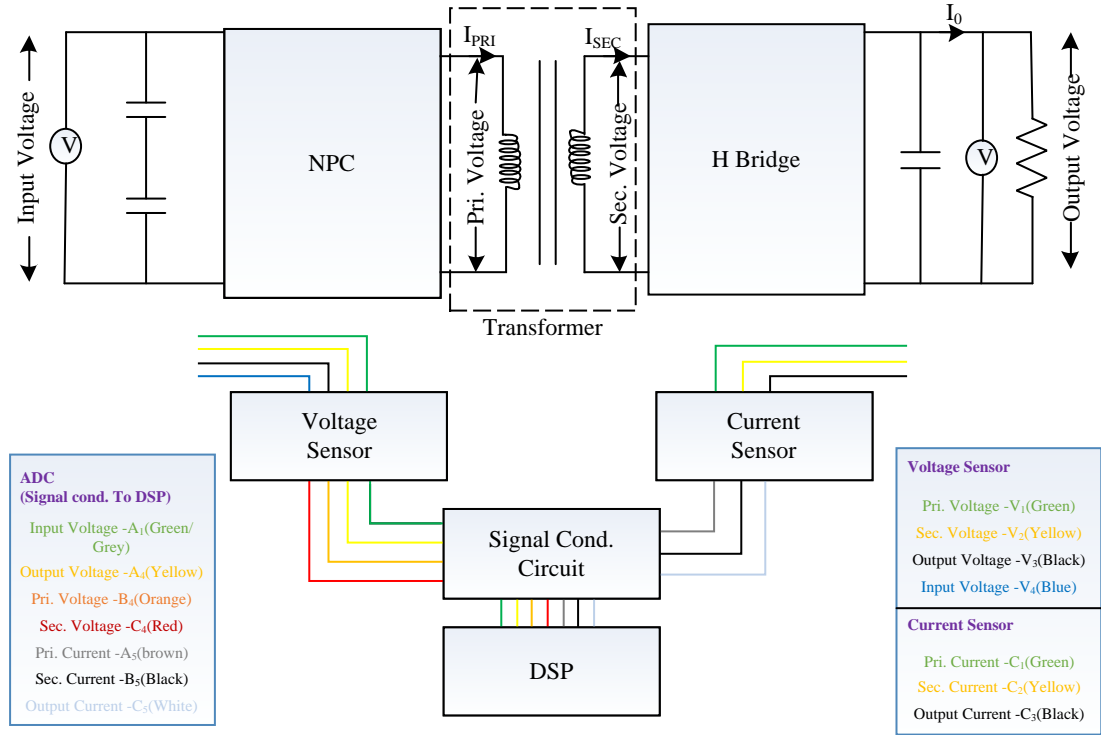


Figure 5.15: Close loop schematic for NPC-DAB converter.

In this setup, the output voltage of the converter must be compared with a reference voltage. This is achieved using the ADC pins of the DSP. The output voltage from the converter is scaled down by a factor of 100 and then sent to a signal conditioning circuit, which converts the waveform from -5 V to $+5\text{ V}$ into a 0 V to 3 V waveform. This conditioned signal is passed through a low-pass filter designed within the DSP.

In the 12-bit ADC (where $3\text{ V} = 2^{12} = 4096$), to remove the 1.5 V offset, the input signal is subtracted by 2048 (i.e., $2^{12}/2$). The resulting value is then multiplied by a gain to make it equivalent to the actual output voltage. This adjusted signal is compared with the reference output voltage value, and the generated result is processed through a PI controller to produce the phase shift ϕ_2 .

In closed-loop hardware, we employ a single-phase shift technique to regulate the output voltage. The reference voltage is set to 20 V . To determine the proportional (P) and integral (I) values for our controller, we used a trial-and-error method. The optimal values found were $P = 0.001$ and $I = 1$.

Initially, the load bank comprised nine loads, each with a resistance of 220 ohms , res-

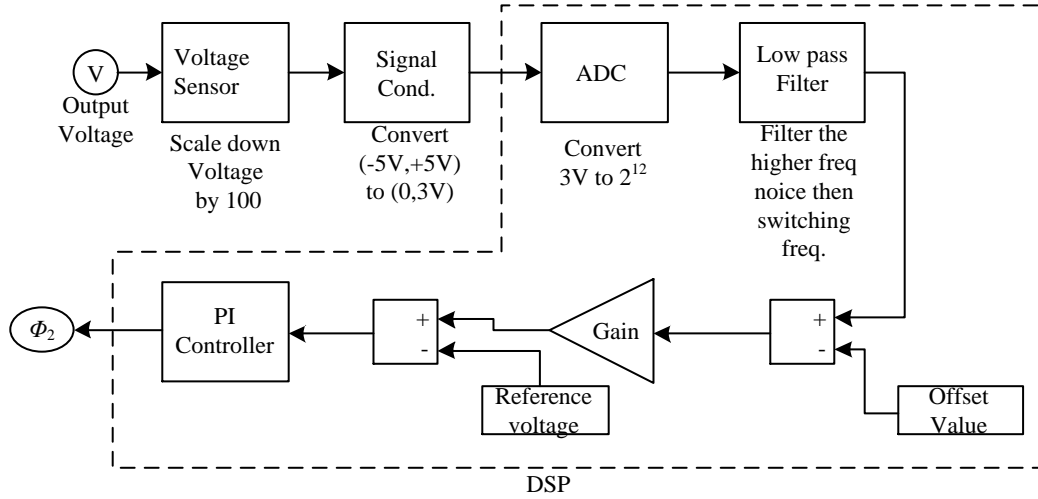


Figure 5.16: Close loop scheme for single phase shift.

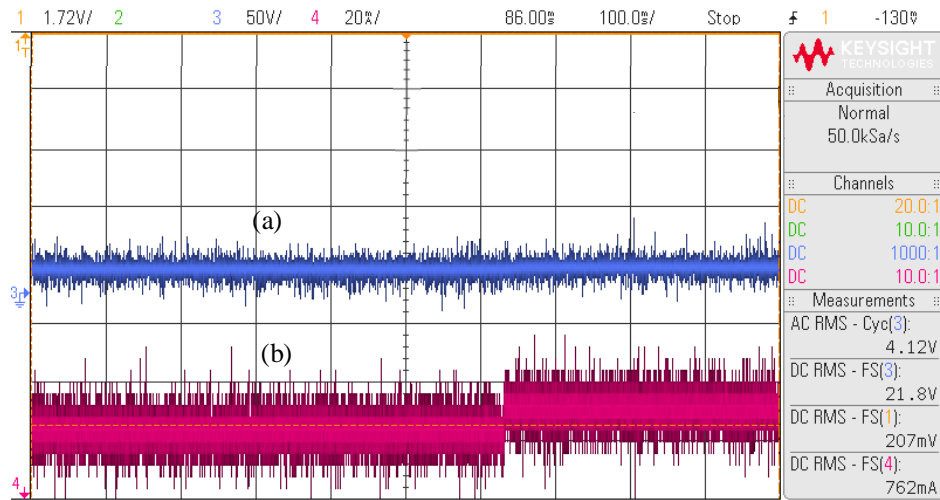


Figure 5.17: (a)Output voltage, (b)Output current.

ulting in an equivalent resistance of approximately 24.4 ohms ($\frac{220}{9} \approx 24.4 \Omega$). During the closed-loop operation, the load was reduced from nine to seven loads, changing the equivalent resistance to approximately 31.42 ohms ($\frac{220}{7} \approx 31.42 \Omega$).

Figure 5.17 illustrates that, despite the variation in load, the output voltage remained constant. This consistency indicates that our converter is successfully operating in a closed-loop configuration.

Chapter 6

Conclusion and Future Scope

6.1 Conclusion

Based on the literature, it is concluded that isolation-based converters are superior to conventional converters for EV charging stations. This project delves into the theoretical analysis of the NPC (Neutral Point Clamped) DAB (Dual Active Bridge) converter, highlighting its advantages over the traditional DAB converter. The study covers both the 4-level and 5-level modes of the NPC DAB converter, providing a comprehensive theoretical examination. To validate these theories, detailed closed-loop and open-loop simulations were conducted using the MATLAB/Simulink framework. These simulations align with the theoretical waveforms, demonstrating a 4-level waveform on the primary side and a 2-level waveform on the secondary side, corresponding to the switching provided.

Following the theoretical and simulation studies, a dedicated NPC PCB submodule was designed to facilitate hardware development. An overvoltage protection circuit was integrated into the NPC submodule. Additionally, a blocking provision was implemented in the NPC submodule to halt the switching pulse when it goes high, used for a software protection mechanism for the NPC.

Finally, the hardware implementation of the NPC DAB converter was realized. Rigorous simulation and experimental tests were carried out under both open-loop and closed-loop conditions to evaluate performance. The waveform revealed a strong correlation between the simulation results and the hardware performance, underscoring the reliability of the proposed designs. This alignment between simulation and experimental data confirms the efficiency and accuracy of the NPC DAB converter. These results highlight the converter's

potential for practical applications, demonstrating significant improvements in performance and reliability.

6.2 Future scope

NPC DAB converters, with their unique blend of features, are finding applications across diverse fields. In the realm of renewable energy, they act as efficient interfaces between solar panels, wind turbines, and the power grid. Their ability to handle bidirectional power flow allows for the seamless injection of renewable energy and utilization of grid power as needed. Furthermore, these converters excel in adjustable speed drives and electric servo motor control applications, providing isolated and adjustable voltage levels for precise motor operation. Additionally, NPC-DAB converters can play a crucial role in grid energy storage systems. They enable bidirectional power flow between storage devices and the grid, ultimately contributing to grid stabilization and the smoother integration of renewable energy sources.

These are just some of the potential applications of NPC-DAB converters. Their versatility and advantageous features make them a valuable technology in various power conversion and management scenarios.

References

- [1] M. Giri and T. B. Isha, “Comparison of non-isolated schemes for ev charging and their effect on power quality,” *2017 International Conference on Circuit ,Power and Computing Technologies (ICCPCT)*, pp. 1–7, 2017.
- [2] S. S. Sayed and A. M. Massoud, “Review on state-of-the-art unidirectional non-isolated power factor correction converters for short-/long-distance electric vehicles,” *IEEE Access*, vol. 10, pp. 11 308–11 340, 2022.
- [3] S. Meikap, C. Kumar, and A. Kumar, “Optimal power management of multi-port converter system in electric vehicle charging station,” in *2022 IEEE 13th International Symposium on Power Electronics for Distributed Generation Systems (PEDG)*, 2022, pp. 1–6.
- [4] S. Meikap, D. Das, C. Kumar, and G. Buticchi, “A multi-port converter system for grid tied electric vehicle charging station,” in *2022 IEEE 13th International Symposium on Power Electronics for Distributed Generation Systems (PEDG)*, 2022, pp. 1–6.
- [5] C. Kumar, R. Zhu, G. Buticchi, and M. Liserre, “Sizing and soc management of a smart-transformer-based energy storage system,” *IEEE Transactions on Industrial Electronics*, vol. 65, no. 8, pp. 6709–6718, 2018.
- [6] S. Falcones, R. Ayyanar, and X. Mao, “A dc–dc multiport-converter-based solid-state transformer integrating distributed generation and storage,” *IEEE Transactions on Power Electronics*, vol. 28, no. 5, pp. 2192–2203, 2013.
- [7] G. P. Adam and B. W. Williams, “Half- and full-bridge modular multilevel converter models for simulations of full-scale hvdc links and multiterminal dc grids,” *IEEE*

Journal of Emerging and Selected Topics in Power Electronics, vol. 2, no. 4, pp. 1089–1108, 2014.

- [8] A. Filba-Martinez, S. Busquets-Monge, J. Nicolas-Apruzzese, and J. Bordonau, “Operating principle and performance optimization of a three-level npc dual-active-bridge dc–dc converter,” *IEEE Transactions on Industrial Electronics*, vol. 63, no. 2, pp. 678–690, 2016.
- [9] A. Verma, K. Mayank, S. Meikap, and C. Kumar, “Modelling and control of modular multilevel converter and dual active bridge based fast electric vehicle charger,” in *2022 4th International Conference on Energy, Power and Environment (ICEPE)*, 2022, pp. 1–6.
- [10] M. S. Tahir, J. Xu, and Y. Wang, “Novel coolmosfet clamping three-level neutral-point-clamping inverter for low and medium power applications,” in *2017 IEEE 3rd International Future Energy Electronics Conference and ECCE Asia (IFEEC 2017 - ECCE Asia)*, 2017, pp. 1949–1953.
- [11] I. T. Akira Nabae and H. Akagi, “New neutral-point-clamped pwm inverter,” 981, *IEEE Transactions on Industry Applications*, pp. 518–519, 1981.
- [12] A. Filbà-Martínez, S. Busquets-Monge, and J. Bordonau, “Modulation and capacitor voltage balancing control of a three-level npc dual-active-bridge dc-dc converter,” in *IECON 2013 - 39th Annual Conference of the IEEE Industrial Electronics Society*, 2013, pp. 6251–6256.
- [13] S. Meikap and C. Kumar, “An npc based triple active bridge isolated converter for fast onboard battery charger for all electric ship,” in *2023 11th National Power Electronics Conference (NPEC)*, 2023, pp. 1–6.
- [14] “How to design a transformer: Size and selection,” 2023. [Online]. Available: <https://eepower.com/technical-articles/how-to-design-a-transformer-size-and-selection/>
- [15] “Launchxl-f28379d overview,” August 2016 – Revised March 2019. [Online]. Available: <https://www.ti.com/product/TMS320F28379D#product-details/>